NASA TECHNICAL NOTE

NASA TN D-5869

NASA TN D-5869
c. 1

DESCRIPTION AND PERFORMANCE OF THE SATURN LAUNCH VEHICLE'S NAVIGATION, GUIDANCE, AND CONTROL SYSTEM

by Walter Haeussermann

George C. Marshall Space Flight Center
Marshall Space Flight Center, Ala. 35812

NATIONAL AERONAUTICS AND SPACE ADMINISTRATION • WASHINGTON, D. C. • JULY 1970

1. REPORT NO. NASA TN D-5869	2. GOVERNMENT ACCESSION NO.	3. RECIPIL
4. TITLE AND SUBTITLE Description and Performance of the Saturn Launch Vehicle's Navigation, Guidance, and Control System		5. REPORT DATE July 1970 6. PERFORMING ORGANIZATION CODE
7. AUTHOR(S)		8. PERFORMING ORGANIZATION REPORT #
9. PERFORMING ORGANIZATION NAME AND ADDRESS George C. Marshall Space Flight Center Marshall Space Flight Center, Alabama 35812		10. WORK UNIT NO. 11. CONTRACT OR GRANT NO.
12. SPONSORING AGENCY NAME AND ADDRESS National Aeronautics and Space Administration Washington, D. C. 20546		13. TYPE OF REPORT & PERIOD COVERED Technical Note 14. SPONSORING AGENCY CODE

15. SUPPLEMENTARY NOTES

Prepared by: Central Systems Engineering
Science and Engineering Directorate

16. ABSTRACT

A review of the navigation, guidance, and control system of the Saturn launch vehicle includes the system analysis and design, signal flow diagrams, redundancy, and self-checking features used to obtain extreme reliability for crew safety.

The iterative path adaptive guidance mode, featuring flight path optimization, is explained and presented in its computational form. Following the analytical considerations, the main guidance and control components are described. The navigation and control information is obtained inertially by a gyro-servo-stabilized, three-gimbal platform system with three mutually orthogonal pendulous-integrating gyro accelerometers; the single-degree-of-freedom gyros as well as the accelerometers use externally-pressurized gas bearings. Rate gyroscopes provide attitude stabilization; some vehicle configurations require additional accelerometer control to reduce wind loads. The digital computer system serves as the computation, central data, and onboard programing center, which ties in with the ground computer system during the prelaunch checkout of the overall system. The control signals are combined, shaped, attenuated, and amplified by an analog type control computer for engine actuator control.

Results from recent launchings of Saturn V vehicles are presented to confirm the adequacy of the navigation, guidance, and control system and its overall performance even under extreme flight perturbations.

17. KEY WORDS Navigation, guidance, and control Optimum guidance Iterative guidance Launch vehicle guidance and control Inertial systems Saturn boosters	18. DISTRIBUTION STATEMENT Unclassified - Unlimited

19. SECURITY CLASSIF. (of this report) Unclassified	20. SECURITY CLASSIF. (of this page) Unclassified	21. NO. OF PAGES 52	22. PRICE* $3.00

*For sale by the Clearinghouse for Federal Scientific and Technical Information
Springfield, Virginia 22151

TABLE OF CONTENTS

LIST OF ILLUSTRATIONS

LIST OF ILLUSTRATIONS (Continued)

LIST OF TABLES

NOMENCLATURE*

$\bar{C}_i$	unit vector normal to the desired elliptical orbit plane.
C_2, C_4	IGM coupling terms for pitch steering.
D_p, D_y	intermediate IGM parameters.
[EPH]	transformation matrix from ephemeral coordinates to earth-centered plumbline coordinates.
F/m	magnitude of the computed acceleration.
f	true anomaly of the predicted cutoff radius vector used in the IGM.
[G]	transformation matrix from earth-centered plumbline coordinates to the desired orbital reference system coordinates.
G_T	magnitude of the desired terminal gravitational acceleration.
i	inclination of the target orbit relative to the equatorial plane.
$J_1, J_2, J_3, J_{12}, J_y, J_p$	intermediate IGM parameters.
K	transformation matrix from earth-centered plumbline coordinates to terminal coordinates.
K_y, K_p	intermediate IGM parameters.
K_{y1}, K_{y2} K_{z1}, K_{z2}	coefficients of the restart guidance yaw and pitch steering equations.
K_i	corrections to the chi-tilde steering angles, i = 1,2,3,4.
K_s	constant used in the calculation of terminal velocity in IGM out-of-orbit precalculations.
$L_1, L_2, L_3, L_{12}, L_3', L_p, L_y$	intermediate IGM parameters.
$\bar{N}$	unit vector normal to the parking orbit plane.
P_1, P_2, P_3, P_{12}	intermediate IGM parameters.
p, p_n	semi-latus rectum of the actual and nominal transfer ellipse, respectively.
$Q_1, Q_2, Q_3, Q_{12}, Q_v, Q_p$	intermediate IGM parameters.
$\bar{R}, R, \bar{R}'$	instantaneous radius vector, vector magnitude, and unit vector, respectively.
$RA\hat{}_T$	right ascension of the target vector.
ROT	control number used to determine whether rotated terminal conditions are used.
$S_1, S_2, S_3, S_{12}, S_y, S_p$	intermediate IGM parameters.
$\bar{S}_1$	unit vector normal to the nodal vector in the elliptical orbit plane.
T_M	magnitude of the minus target vector.
T_T, T_T'	corrected and estimated total time-to-go.
T_x, T_y, T_z	components of the unit target vector $\bar{T}$ in ephemeral coordinates.
$\bar{T}_p$	unit target vector in earth-centered plumbline coordinates.
T_{1c}	burn time of the IGM first, second, and coast guidance stages.
T_3, T_3'	corrected and estimated time remaining in the third or fifth stages of IGM guidance.
$\Delta T_4, \Delta T_4'$	actual difference and limited difference, respectively, between actual burn time and nominal burn time of the S-IVB first burn.
t_D	time into launch window.
U_1, U_2, U_3, U_{12}	intermediate IGM parameters.
V, V_T	actual velocity and desired terminal velocity, respectively.
X_S, X_S, Z_S	position components in the earth-centered pumbline system.
X_{S1}, Y_{S1}, Z_{S1}	direction cosines of the thrust vector in the earth-centered pumbline system.
X_1, X_2	intermediate values.
X_4, Y_4, Z_4	position components in orbit reference system.
α_D	angle from the perigee vector to the descending nodal vector measured positive in the direction of flight.
$\alpha_{TS}, \alpha^*_{TS}$	desired angle and nominal angle between the $\bar{S}$ and $\bar{T}_p$ at reignition, respectively.
δ_2	intermediate IGM parameter.
(ξ, η, ζ) (ξ_T, η_T, ζ_T)	instantaneous position components and desired terminal position components in the terminal reference system, respectively.
$\Delta\xi, \Delta\eta$	position components to be gained along ξ and η axes, respectively.
$\Delta\dot{\xi}, \Delta\dot{\eta}, \Delta\dot{\zeta}$	velocity to be gained along ξ, η, ζ axes.
$\Delta\xi', \Delta\eta', \Delta\zeta'$	intermediate velocity deficiency used in estimating time-to-go.

*See Table 2 for additional definitions.

NOMENCLATURE (Continued)

$(\ddot{\xi}_G, \ddot{\eta}_G, \ddot{\zeta}_G)$, $(\ddot{\xi}_{GT}, \ddot{\eta}_{GT}, \ddot{\zeta}_{GT})$	instantaneous and terminal gravitational components in the terminal reference system, respectively.
θ_N	descending nodal angle of target orbit measured counterclockwise from the launch meridian in the equatorial plane.
γ, γ_T	instantaneous and desired terminal flight path angle, respectively, measured positive counterclockwise from the local horizontal.
σ	angle between perigee vector and target vector in the nominal transfer ellipse.
ϕ_T	angle used to estimate the location of the terminal radius vector in the desired orbit plane, measured positive clockwise from the positive X_4-axis.
χ_{Yi}, χ_{Zi}	pitch and yaw attitude steering angles.
$\tilde{\chi}_Y, \tilde{\chi}_Z$	pitch and yaw steering angles required to null out the velocity deficiencies in the remaining estimated flight time, without regard to terminal radius measured in the ξ, η, ζ coordinate system.
χ_Y'', χ_Z''	IGM computed pitch and yaw angles as measured in the ξ, η, ζ coordinate system.
ψ'	angle between the $\bar{S}$ and $\bar{T}_p$ at S-IVB reignition.
First stage	from initiation of IGM calculations after S-II stage ignition until the propellant mixture ratio change occurs.
Second stage	from the time the mixture ratio change occurs until S-II cutoff.
Third stage	S-IVB stage burn into orbit.
Fourth stage	from after S-IVB reignition until the propellant mixture ratio change occurs.
Fifth stage	from the time the mixture ratio change occurs until S-IVB second cutoff.

DESCRIPTION AND PERFORMANCE OF THE SATURN LAUNCH VEHICLE'S NAVIGATION, GUIDANCE, AND CONTROL SYSTEM

SUMMARY

A review of the navigation, guidance, and control system of the Saturn launch vehicle includes the system analysis and design, signal flow diagrams, redundancy, and self-checking features used to obtain extreme reliability for crew safety.

The iterative path adaptive guidance mode, featuring flight path optimization, is explained and presented in its computational form. Following the analytical considerations, the main guidance and control components are described. The navigation and control information is obtained inertially by a gyro-servo-stabilized, three-gimbal platform system with three mutually orthogonal pendulous-integrating gyro accelerometers; the single-degree-of-freedom gyros as well as the accelerometers use externally-pressurized gas bearings. Rate gyroscopes provide attitude stabilization; some vehicle configurations require additional accelerometer control to reduce wind loads. The digital computer system serves as the computation, central data, and onboard programming center, which ties in with the ground computer system during the prelaunch checkout of the overall system. The control signals are combined, shaped, attenuated, and amplified by an analog type control computer for engine actuator control.

Results from recent launchings of Saturn V vehicles are presented to confirm the adequacy of the navigation, guidance, and control system and its overall performance even under extreme flight perturbations.

INTRODUCTION

The missions of large launch vehicles comprise manned flights as well as unmanned flights. For these flights, it is not economically feasible to use different guidance and control systems; therefore, the same system must fulfill the various operational requirements necessary to meet the severe combinations of accuracy, reliability, and lifetime. For vehicles with nonrecoverable booster stages, a single guidance and control system must accomplish all the requirements. The present technology solves the control problems of the different flight phases by discrete, preprogramed operating modes rather than by self-adapting or learning methods as foreseeable in future systems.

In the following review, the guidance and control system of the Saturn class launch vehicles is used as a typical example for the design requirements and the solutions to obtain an optimal system that guides and controls the multistage launch vehicle.

LAUNCH VEHICLE FLIGHT PHASES

Aerodynamic pressure (Q), acceleration (F/m), and velocity (V_S) for a typical three-stage Saturn V flight trajectory into earth orbit are shown in Figure 1. During the first stage flight, the vehicle traverses the high aerodynamic pressure region. Structural loads from aerodynamic forces are kept as small as possible by controlling the vehicle with a minimum angle of attack; therefore, in this first stage flight, a standard tilt program is used and guidance corrections are not introduced before the early part of the second stage flight. For attitude stabilization, attitude control signals from the inertial platform stabilized by three orthogonally-arranged single-degree-of-freedom gyros and angular rate signals derived from rate gyroscopes are used; in specific cases, control accelerometers can generate additional attitude control commands. The actual shaping of these signals and their application will be described later.

An iterative guidance mode for flight path adaptive guidance has been developed to guide the vehicle along a minimum propellant trajectory to fulfill the desired orbital or transearth conditions. The guidance system determines the crossrange flight path corrections and the proper cutoff commands to obtain the required velocity vector for the flight vehicle.

ITERATIVE PATH ADAPTIVE GUIDANCE MODE

The optimizing techniques of the calculus of variations were used to develop the iterative path adaptive guidance mode. Experience with hundreds of minimum propellant trajectories for various orbital injection missions has demonstrated that the optimum thrust direction relative to the local vertical is very nearly a linear function of time during vacuum flight. Moreover, the size of the angle between the optimum thrust direction and the local horizon is never very large for an orbital mission (Fig. 2). These observations show a remarkable agreement with the mathematical results obtained from the calculus of variations when a flat earth model having a constant gravitational field is used and position and velocity constraints are imposed at cutoff. A closed solution, which

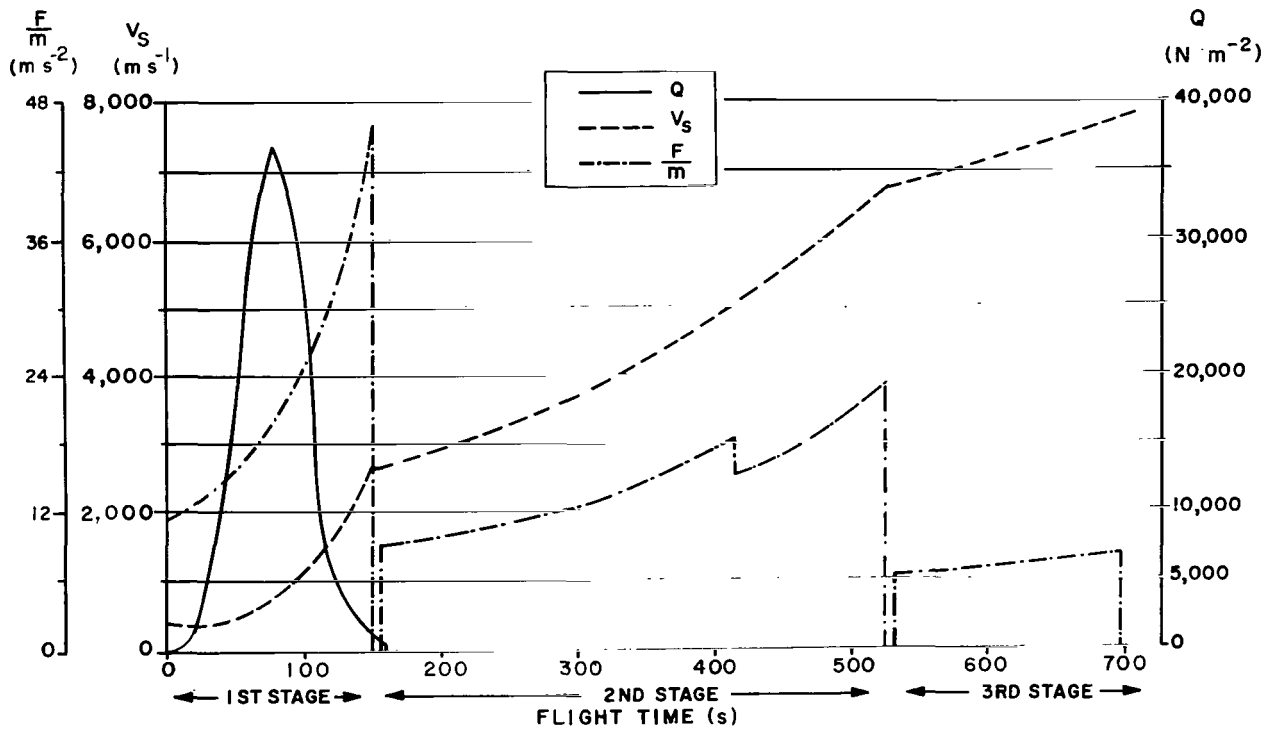

FIGURE 1. ACCELERATION, VELOCITY, AND AERODYNAMIC PRESSURE FOR A TYPICAL SATURN V TRAJECTORY.

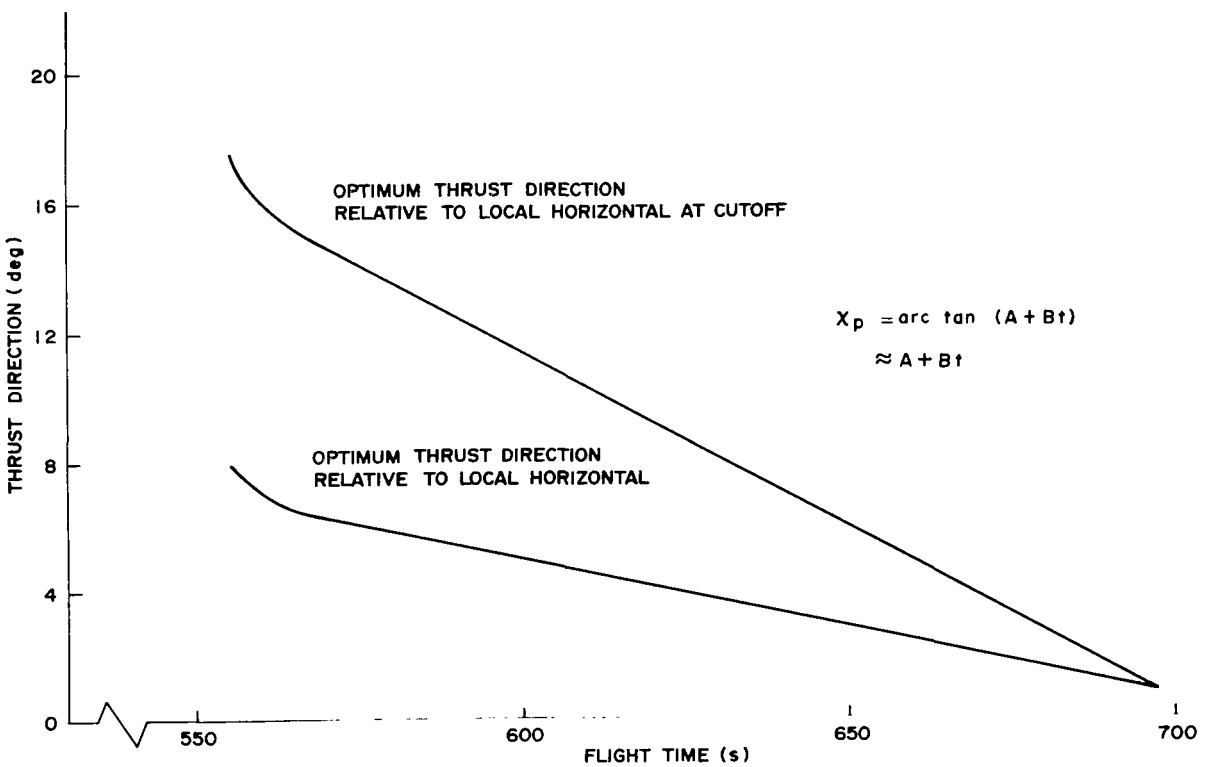

FIGURE 2. OPTIMUM THRUST ANGLE PROFILE.

can be obtained with this mathematical model, yields an explicit equation for the optimum thrust direction.[1] This equation has the form

$$\chi_p = \arctan (A + Bt) \qquad (1)$$

where χ_p is the optimum thrust direction for minimum propellant consumption. Constants A and B are determined by the specified cutoff velocity and position, the initial values of the state variables, the vehicle thrust acceleration, and the engine specific impulse. The comparison of this equation with the results of trajectory studies suggests the use of the approximation

$$\chi_p = A + Bt. \qquad (2)$$

A guidance coordinate system (X_V, Y_V, Z_V) (Figs. 3 and 4) is established with the origin at the center of the earth and with the X_V axis lying along the vertical which intersects the calculated cutoff position of the vehicle. Simplified equations of motion are derived to approximate the motion over an oblate earth with a realistic gravitational field. These equations of motion are solved during flight to determine the instantaneous range angle to cutoff, the time-to-go to cutoff, and the gravitational effects occurring over the remaining flight time. This information is used to compute values for A and B continuously during flight except near cutoff.

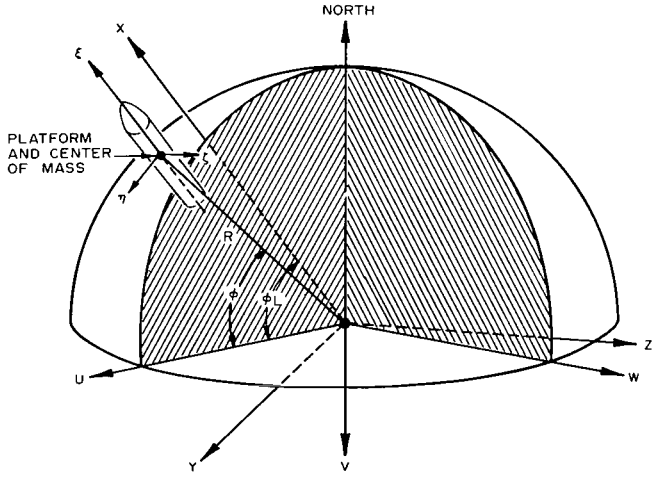

φ_L Geodetic latitude of launch site.

(X, Y, Z) Space-fixed coordinate system for guidance computations with its origin at the earth's center. The X and Z axes define the flight plane.

(ξ, η, ζ) Inertial coordinate system established by the orientation of the accelerometers on the stabilized platform and parallel to the X, Y, Z system at launch.

(U, V, W) Space-fixed coordinate system with its origin at the earth's center. The U-V plane contains the launch point.

FIGURE 3. GUIDANCE COORDINATE SYSTEMS.

(X,Z) = SPACE-FIXED NAVIGATION COORDINATE SYSTEM
(X_v,Z_v) = SPACE-FIXED GUIDANCE COORDINATE SYSTEM

SUBSCRIPTS:
i = INSTANTANEOUS VALUES
c = TERMINAL VALUES
v = GUIDANCE COORDINATE VALUES

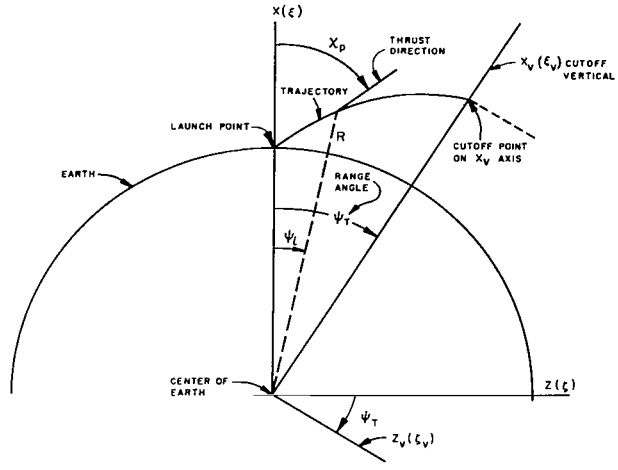

FIGURE 4. COORDINATE SYSTEM OF THE ITERATIVE GUIDANCE SCHEME.

Special procedures are required during the last several seconds before cutoff because the equations give an indeterminate command angle at the cutoff point. This procedure is established as follows: the quantity A may be expressed as the sum of a function of velocity, A (V), and a function of altitude, A (h). Near cutoff, the altitude term will require very large command angles even for small altitude errors. Since the vehicle attains the desired altitude before the desired cutoff velocity is reached, the altitude term may be dropped from the calculations several seconds before cutoff without degrading the injection accuracy. Moreover, the rate term, B, is not needed because the vehicle turning rate is small and nearly constant; this term may also be dropped from the calculations without penalty. The altitude constraint and the rate term are presently dropped in the Saturn V flight program at approximately 46 seconds before cutoff. The resulting steering law is termed the chi tilde mode. A further improvement is accomplished in the cutoff region by freezing the command angles at approximately 8 seconds before cutoff. A representative set of equations is shown in Tables 1 and 2.[2] A simple velocity presetting is used to initiate engine cutoff going into earth orbit, and an energy equation is used to effect engine cutoff for injection into lunar trajectory.

Table 1a. IGM Navigation and Guidance into Earth Orbit

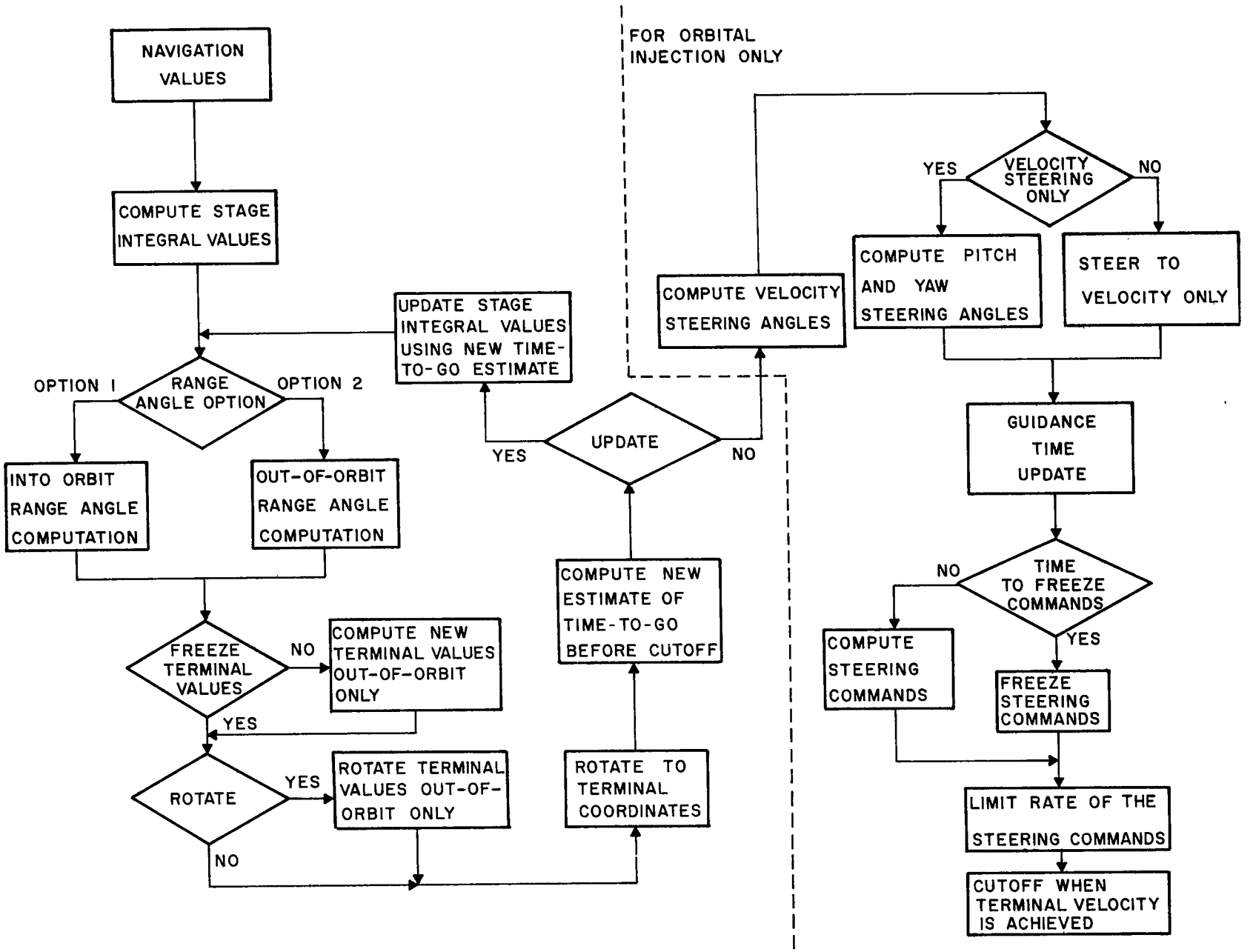

Table 1b. Iterative Guidance Mode Equations

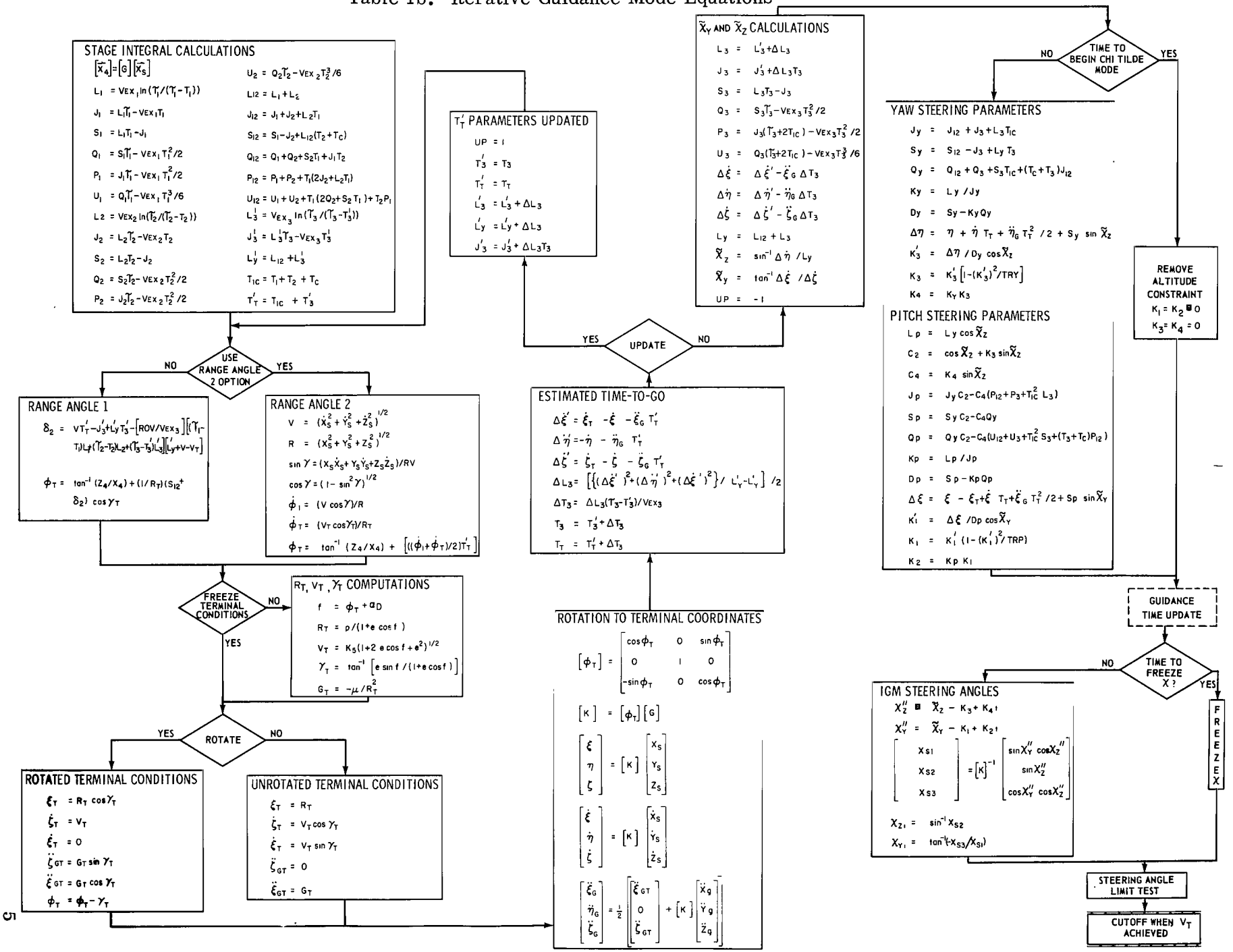

Table 2a. Guidance Inputs and Out-of-Orbit Guidance

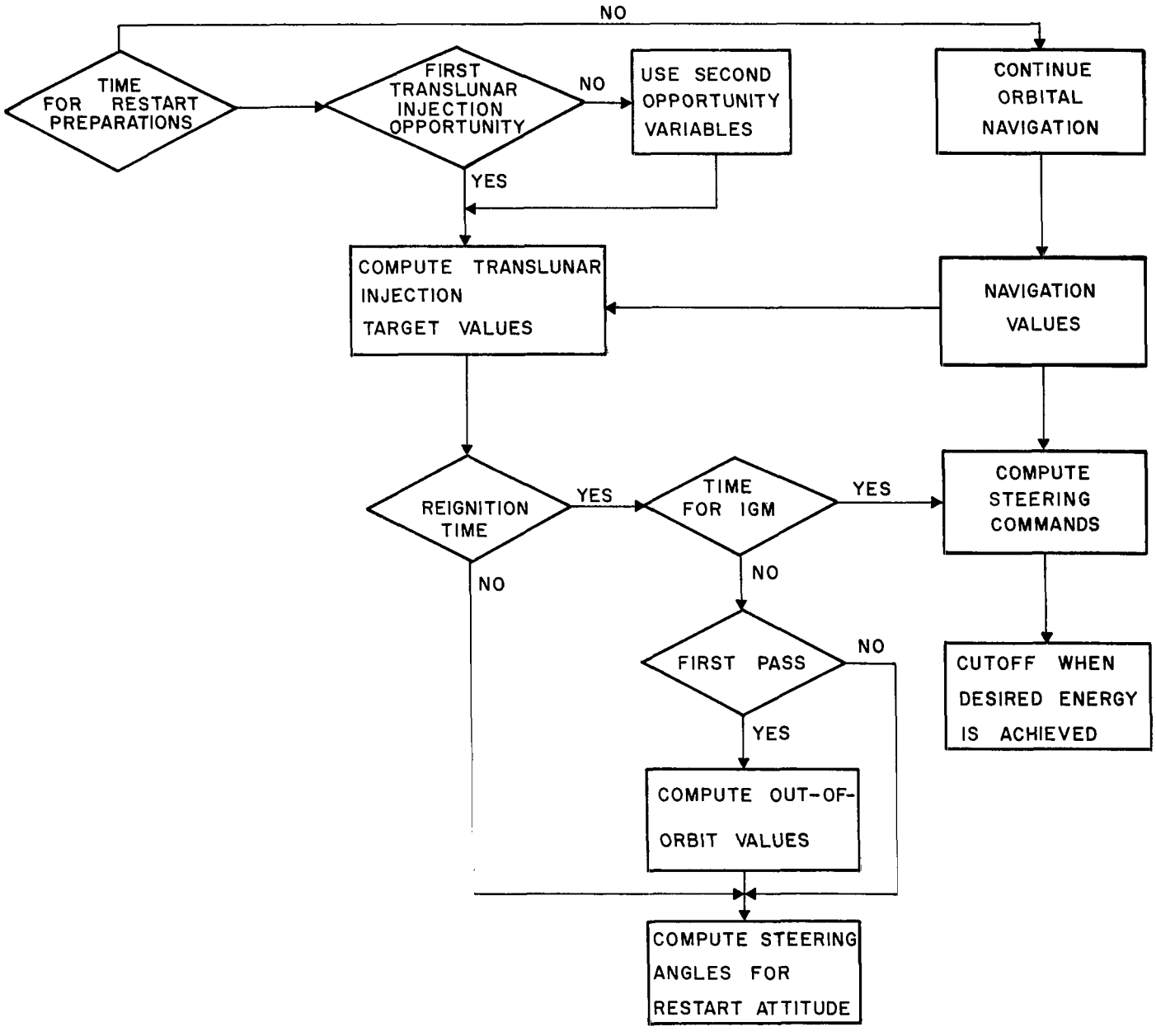

Table 2b. Guidance Inputs and Out-of-Orbit Guidance

DEFINITIONS			
p	= SEMI-LATUS RECTUM OF THE TERMINAL ELLIPSE.	$\bar{S}$	= NODAL VECTOR.
μ	= PRODUCT OF UNIVERSAL GRAVITATIONAL CONSTANT AND EARTH MASS.	e	= ECCENTRICITY OF THE TRANSFER ELLIPSE.
$\bar{T}$	= TARGET VECTOR IN EPHEMERAL COORDINATES.	e_n	= ECCENTRICITY OF THE NOMINAL TRANSFER ELLIPSE

INPUTS FOR BOOST-TO-ORBIT			
T_1	= TIME REMAINING IN THE FIRST STAGE OF IGM GUIDANCE.	T_3'	= TIME REMAINING IN THIRD OR FIFTH STAGE BURN.
T_2	= TIME REMAINING IN THE SECOND STAGE OF IGM GUIDANCE.	T_C	= COAST TIME BETWEEN S-II BURNOUT AND S-IVB IGNITION.
V_{ex1}	= EXHAUST VELOCITIES FOR FIRST STAGE OF IGM.	T_{4N}	= NOMINAL TIME IN 3RD IGM STAGE.
V_{ex2}	= EXHAUST VELOCITIES FOR SECOND STAGE OF IGM.	R_T	= DESIRED TERMINAL RADIUS.
V_{ex3}	= EXHAUST VELOCITIES FOR THIRD STAGE OF IGM.	V_T	= DESIRED TERMINAL VELOCITY.
τ_1	= ESTIMATED TIME TO DEPLETE VEHICLE MASS BEFORE SECOND MRS.	γ_T	= DESIRED TERMINAL FLIGHT PATH ANGLE.
τ_2	= ESTIMATED TIME TO DEPLETE VEHICLE MASS FROM MRS TO STAGE CUTOFF.	$A_{\bar{z}}$	= $\sum \text{Ln}(T_L - T_{LO})^n$. $N = 4$ $N = 0$
τ_3	= ESTIMATED TIME TO DEPLETE S-IVB MASS.	T_L	= LIFTOFF TIME.
		T_{LO}	= OPENING OF LAUNCH WINDOW.
		ϕ_L	= GEODETIC LATITUDE OF THE LAUNCH SITE.

INPUTS FOR OUT-OF-ORBIT			
ϵ_{2R}	= CONSTANT TIME FOR SELECTION OF GUIDANCE OPTION WHICH ENFORCES ONLY TERMINAL VELOCITY END CONDITIONS DURING S-IVB SECOND BURN.	β, β'	= CONSTANT ANGLE DEFINING THE LOCATION OF THE PSEUDO NODAL ($\bar{S}$) VECTOR WITH RESPECT TO THE RADIUS VECTOR IN THE IGNITION PLANE AT S-IVB RESTART PREPARATION TIME FOR 1st & 2nd OPPORTUNITIES, RESPECTIVELY.
ϵ_{1R}	= CONSTANT TIME FOR SELECTION OF GUIDANCE OPTION WHICH ALLOWS AN ALTERNATE COMPUTATION OF THE TERMINAL RANGE ANGLE DURING S-IVB SECOND BURN.	β_1, β_1'	= CONSTANT ANGLE DEFINING THE LOCATION OF THE NODAL ($\bar{S}$) VECTOR WITH RESPECT TO THE RADIUS VECTOR IN THE IGNITION PLANE AT S-IVB REIGNITION OF 1st & 2nd OPPORTUNITIES, RESPECTIVELY.
ϵ_{3R}	= CONSTANT TIME FOR SELECTION OF GUIDANCE WHICH FREEZES THE TERMINAL CONDITIONS DURING THE SECOND S-IVB BURN.	α_{TS}^*	= THE NOMINAL PLANE ANGLE BETWEEN THE ($\bar{S}$) & $\bar{T}_D$ VECTORS AT REIGNITION.
K_{en}	= CONSTANT TO UPDATE ECCENTRICITY FOR SECOND OPPORTUNITY INJECTION.	T_{2R}	= NOMINAL 4th STAGE BURN TIME.
$\dot{M}_{2R}$	= MASS FLOW RATE OF S-IVB PRIOR TO MRS DURING SECOND BURN.	T_{3R}'	= ESTIMATE 5th STAGE BURN TIME.
$\dot{M}_{3R}$	= MASS FLOW RATE OF S-IVB AFTER MRS DURING SECOND BURN.	ϕ_{TR}	= INITIAL ESTIMATE AT THE LOCATION OF THE TERMINAL RADIUS VECTOR FOR S-IVB SECOND BURN.
ROVR	= CONSTANT FOR BIASING THE TERMINAL RANGE ANGLE PREDICTION DURING S-IVB SECOND BURN.	τ_{3R}	= ESTIMATED TIME TO DEPLETE VEHICLE MASS IN THE SECOND BURN OF S-IVB.
TRPR,TRYR	= CONSTANTS USED TO BIAS THE PITCH & YAW STEERING PARAMETERS DURING S-IVB SECOND BURN.	F_{NR}	= NOMINAL THRUST AT S-IVB REIGNITION.
V_{ex2r}	= EXHAUST VELOCITIES FOR 4th & 5th	$K_{\alpha 1}$, $K_{\alpha 2}$	= COEFFICIENTS OF POLYNOMIAL DEFINING THE ANGLE α_{TS}.
V_{ex3r}	= STAGES OF IGM.	R_N	= RADIUS AT NOMINAL S-IVB REIGNITION
M_{NR}	= MASS OF VEHICLE AT THE NOMINAL S-IVB REIGNITION POINT.	$RA_T^{\uparrow}$	= RIGHT ASCENSION OF THE LAUNCH SITE.
		$DEC_T^{\uparrow}$	= DECLINATION OF LAUNCH SITE.
		C_3	= ENERGY OF THE DESIRED TRANSFER ELLIPSE.
		COS α	= COSINE OF THE ANGLE BETWEEN THE PERIGEE & TARGET VECTORS IN THE NOMINAL TRANSFER ELLIPSE.

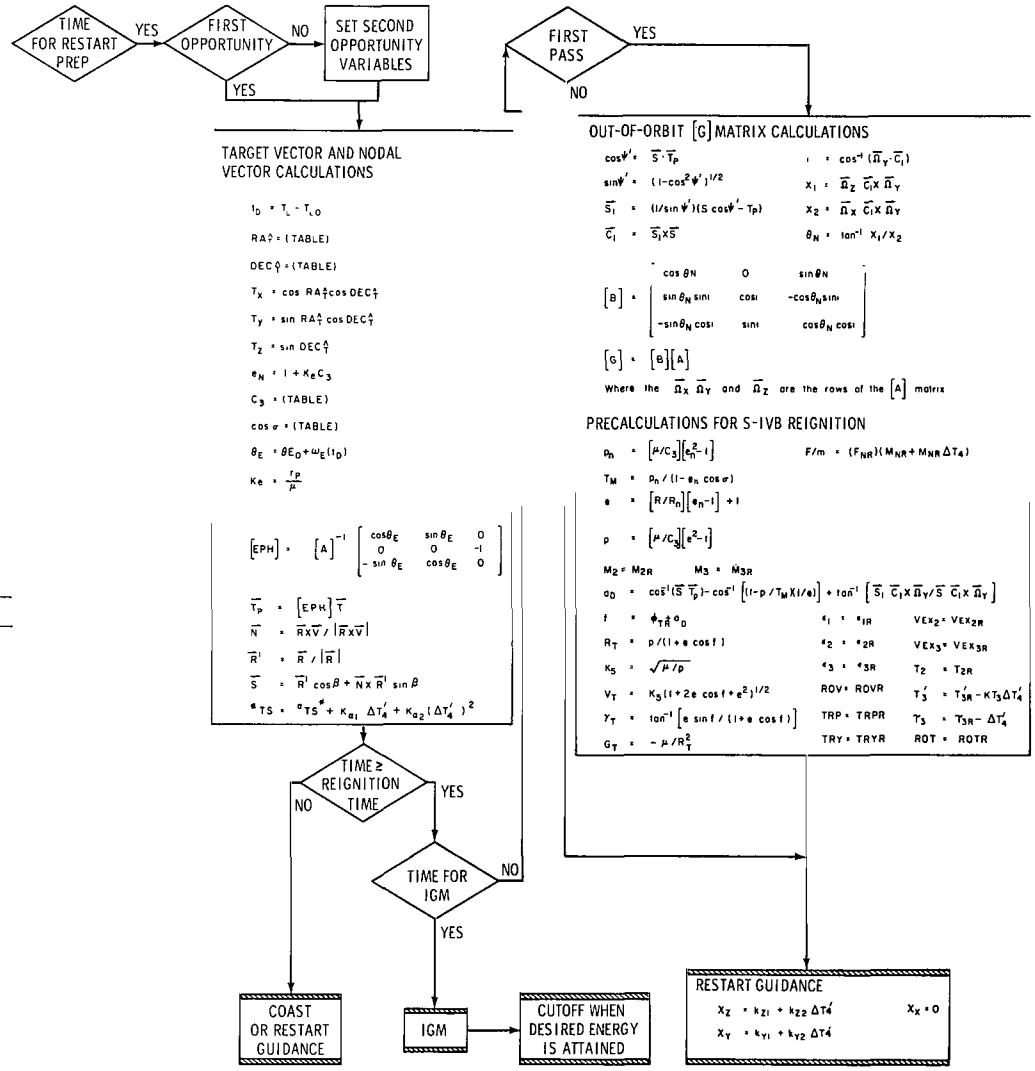

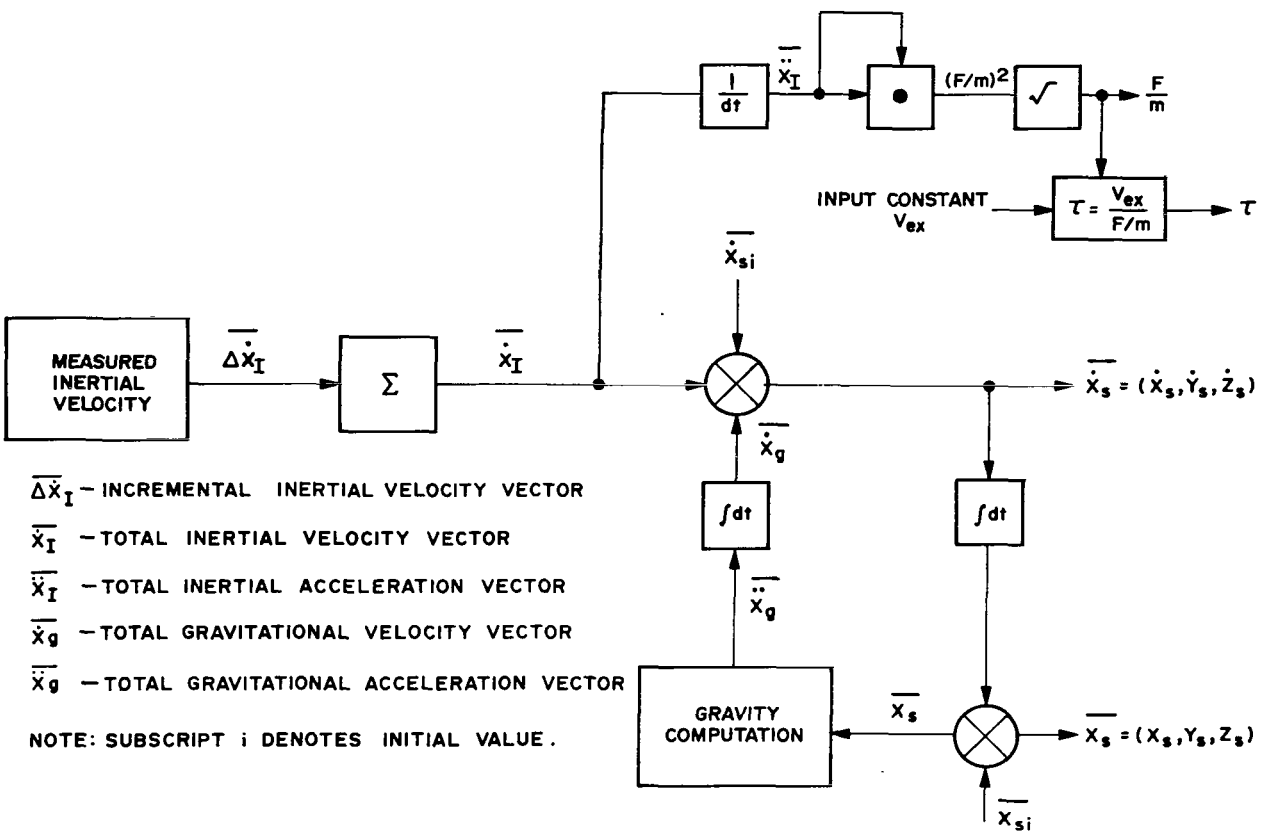

FIGURE 5. MEASURED VALUES AND NAVIGATION COMPUTATIONS.

The guidance system requires inputs from the navigation system to compute the thrust direction command. Figure 5 shows the process by which the inputs to the guidance equations are determined. Inertial velocity caused by thrust and aerodynamic forces acting on the vehicle is measured by accelerometers mounted on the inertial platform. The readings are processed in the accelerometer processing routine where they undergo reasonableness tests to determine the accelerometer outputs to be used. After the inertial velocity is obtained, these values are used in the navigation calculations to compute the inputs required in the guidance equations. These inputs are the vehicle state vector (position and velocity vector), the vehicle inertial acceleration magnitude, and a measure of the time, τ, necessary to burn the complete vehicle (assuming a constant mass flow rate and thrust).

LAUNCH VEHICLE CONTROL

Introduction to Launch Vehicle Control Problems

During propulsion, the attitude control system must appropriately orient the thrust vector relative to the vehicle such that the required attitude commands are performed in a satisfactorily damped mode of rotation. Problems in vehicle control arise because Saturn vehicles cannot be considered rigid but must be treated as distributed masses connected by an elastic structure. Forces acting on these masses resulting from atmospheric perturbations or active control of the vehicle excite the complex spring-mass system and cause body bending. Since the structure possesses low damping, oscillatory bending modes of considerable amplitude can be produced; the control sensors may be subjected

to these large amplitude oscillations at their particular location. Thus incorrect information about the total vehicle behavior may cause self-excitation and instability of the vehicle control system.

Another problem is that the vehicles are aerodynamically unstable during most of the propelled flight in the atmosphere. As an example, Figure 6 is a plot of the center of pressure and the center of mass for the first phase of the Saturn V and shows that the vehicle is unstable except for a short period of time around the 60th flight second.

The control system designer must consider that propellant sloshing exerts low frequency forces on the vehicle, and excitation through the control loop must be prevented. Also many vehicle characteristic data vary widely with time and the individual propulsion stages;

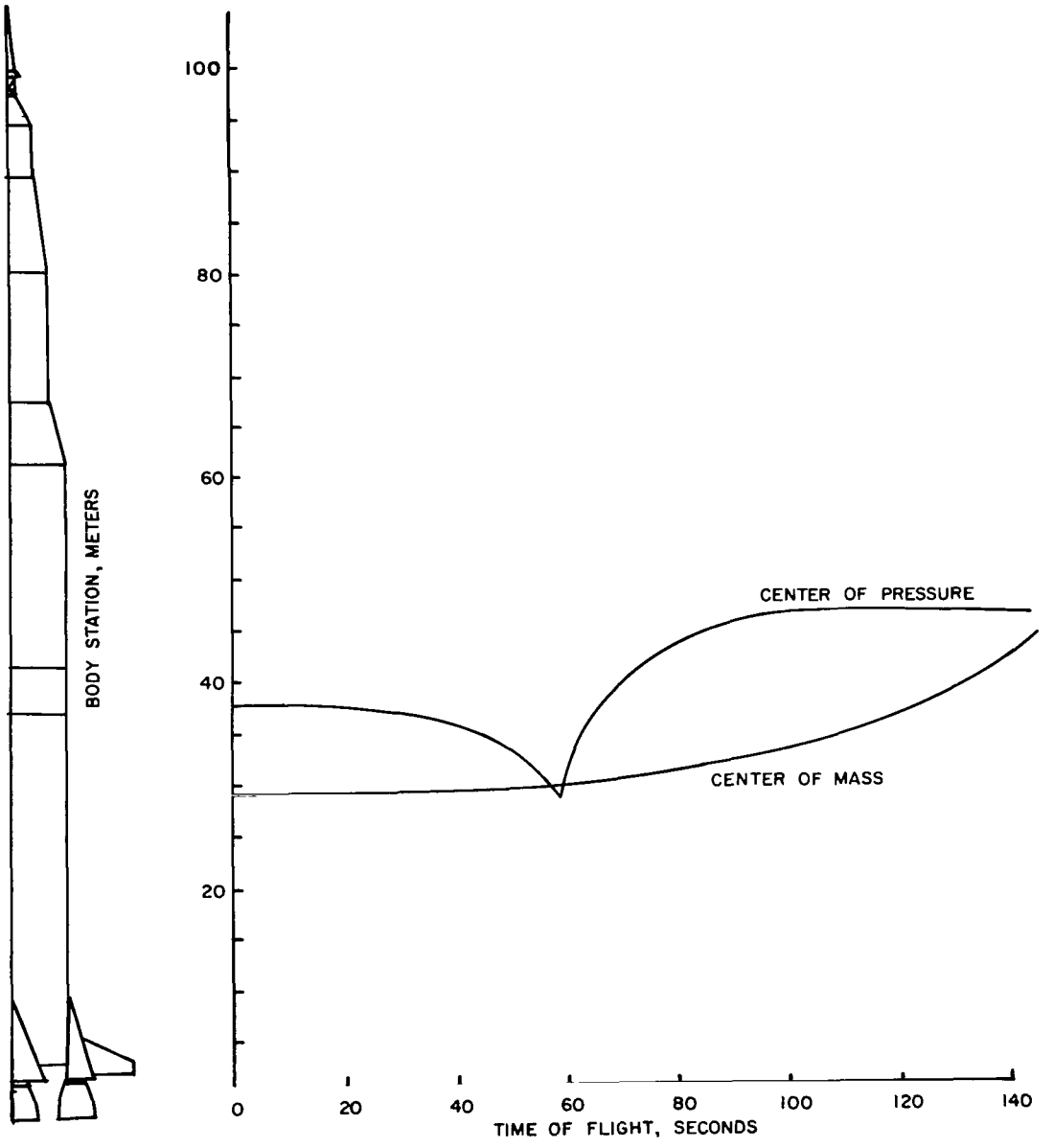

FIGURE 6. VARIATIONS OF CENTER OF PRESSURE AND CENTER OF MASS DURING FLIGHT.

some can be predetermined only to a certain degree and tolerances must be imposed. Thus a comparatively wide operating range of the control system must be provided.

Vehicle Motion Equations[3]

For the control system synthesis and analysis, the vehicle motions must be available in the form of equations that serve as a mathematical model.

In establishing the equations, it is assumed that certain characteristic data can be treated as constants or slowly time varying functions and do not influence the characteristic modes of the control system for the time interval under investigation. Furthermore, terms of a negligible influence to the practical results are omitted.

The basic vehicle dynamics for small perturbations involve five ordinary linear differential equations.

1. Moment balance equation for the rigid-body vehicle, coupled with sloshing mass and engine mass reactions.

2. Force balance equation for the rigid-body vehicle, coupled with sloshing mass and engine mass reactions.

3. Bending mode equations for the disturbed elastic vehicle structure, coupled with sloshing mass and engine mass reactions.

4. Force balance equations for the propellant sloshing masses, coupled with rigid-body and elastic reactions.

5. Angular relationships between rigid-body dependent variables.

In addition to these basic vehicle dynamics, other equations are introduced to define the dynamics of the control logic, engine, actuators, and control sensors.

Control Scheme and Equations

The development of the control scheme and its equations demands investigations in two areas: one covers the low frequency spectrum, consisting of the rigid-body control frequency and propellant sloshing; and the other covers the high frequency spectrum, consisting primarily of the bending modes, torsional modes, and compliance modes. After both areas have been analyzed, the effect of cross-coupling is examined and any necessary adjustments in the system are made. The complexity of the frequency spectrum as it exists, for example on the Saturn V, can be seen in Figure 7, which shows the basic frequencies during the first powered phase. The frequency bands are the results of changing vehicle state conditions because of propellant consumption as a function of flight time.

An attitude/attitude-rate control scheme is used for the Saturn V. This control technique in conjunction with a wind-biased tilt program has proven adequate in maintaining structural loads within acceptable limits. Should a structural load relief become necessary for more unfavorable center of pressure to center of mass configurations, accelerometer control will be added to the attitude/attitude-rate control.

The control law for an engine deflection β is

$$\beta = a_o \Delta\phi + a_1 \dot{\phi} + [g_2 \ddot{\gamma}] \tag{3}$$

where $\Delta\phi$ and $\dot{\phi}$ are the attitude error angle and the attitude rate and $\ddot{\gamma}$ is the lateral acceleration measured by a body-mounted accelerometer with its sensitive axis perpendicular to the vehicle longitudinal axis; a_o, a_1, and g_2 are gain factors which must be properly selected to produce the drift-minimum or load-minimum condition.

If necessary, control accelerometers will be rigidly attached to the vehicle to measure the acceleration normal to the vehicle axis. The acceleration measured by this control accelerometer differs from that measured by the guidance accelerometers, which are mounted on the stable platform and measure accelerations with respect to an inertial space coordinate system. In simplified mathematical terms, the acceleration sensed by such a control accelerometer is

$$\ddot{\gamma} = \frac{N'}{m}\alpha + \frac{R'}{m}\beta + l_a \ddot{\phi} \tag{4}$$

where the first term is the partial acceleration from an angle of attack, the second term results from the deflected thrust vector, and the third term is derived from the angular vehicle acceleration with l_a defined as the distance between the vehicle center of mass and the body-mounted accelerometer.

The design and selection of the control parameters for low frequency response are determined by consideration of several factors, such as:

1. The rigid-body control frequency should be sufficiently below the frequency of the lowest bending mode to allow the design of shaping networks that stabilize the bending modes without adversely affecting the control mode.

2. The control frequency must be high enough to provide adequate vehicle response and to minimize trajectory dispersions caused by thrust vector misalignment.

3. The control gains, which determine the control frequency, must be high enough to guarantee that the operating point does not go below the static stability margin when tolerances in coefficients are included.[4]

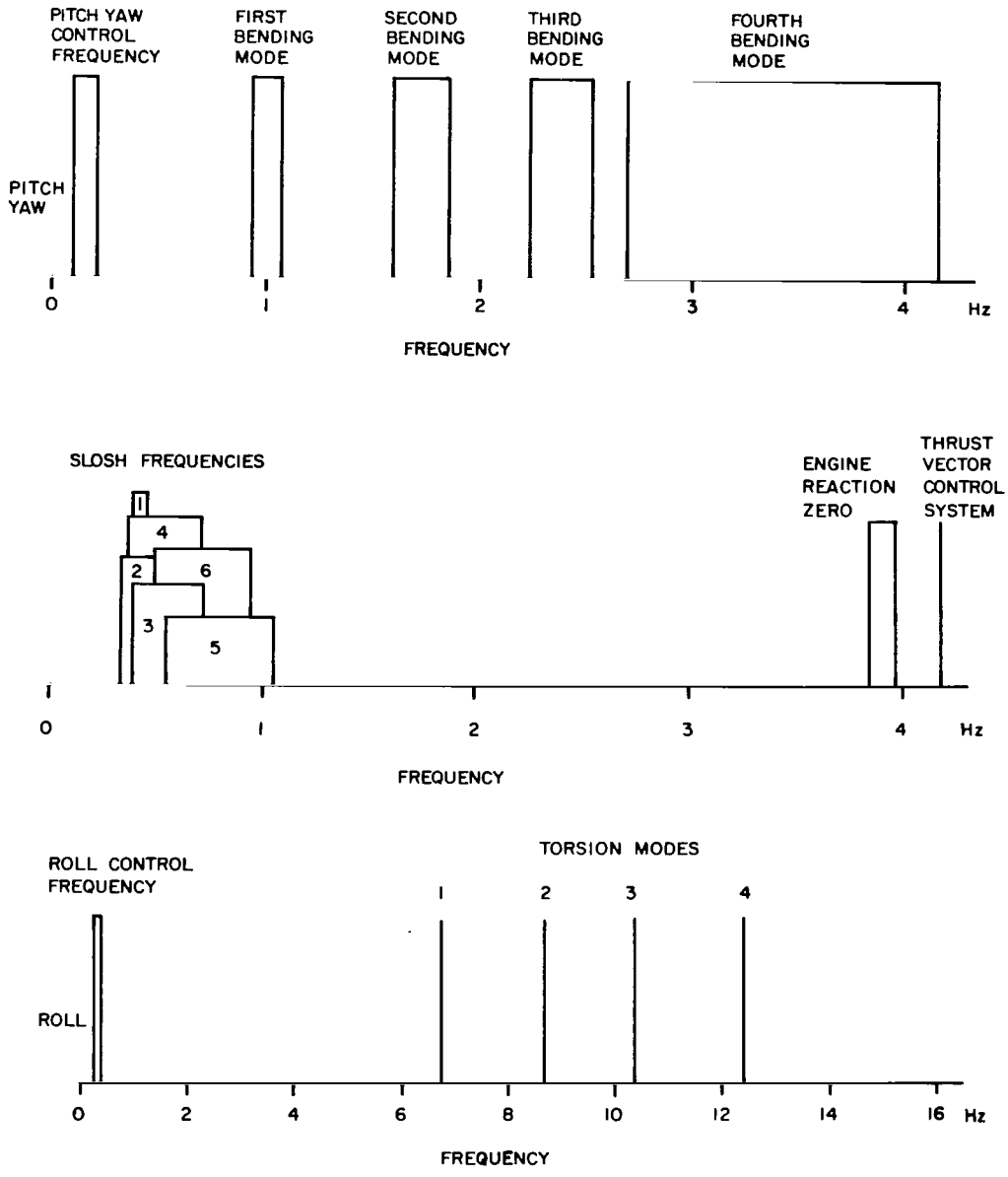

FIGURE 7. FREQUENCY SPECTRUM DURING FIRST STAGE PROPULSION.

Typical tolerances used in designing the Saturn control systems are as follows.

1. ±0.2 caliber variation in the center of pressure location.
2. ±6% of the normalized force coefficient $c_{z\alpha}$.
3. ±0.15 caliber variation in the vehicle center of mass.
4. ±10% variation in the control gains.
5. ±3% variation in engine thrust and/or loss of the thrust of one or even two engines after certain burning times for multiple engine systems.

To some degree, requirements 1, 2, and 3 are too rigid in their extreme value combination, and the selection of the control frequency requires considerable evaluation and compromise before the final values are obtained. During the first propulsion phase, the control frequency chosen ranges from 0.08 to 0.2 Hz. Simulator studies indicate that these values give reasonable dynamic response while lower values cause undesirably large dispersions in case of thrust vector misalignment and other system errors. The control frequency for the second stage burn is also approximately 0.15 Hz; however, this value was chosen mainly in view of first and second stage separation dynamics.[5] The third stage control frequency ranges between 0.2 and 0.5 Hz.

The selected control frequencies determine the control loop gains. Typical gain values for the Saturn V launch vehicles are given in Table 3. Changes in the attitude and attitude-rate gain for all stages will be by discrete steps as a function of flight times. These changes are necessary to adjust to changing vehicle characteristics as propellant is consumed.

Damping with respect to the sloshing modes is obtained by providing baffles in the propellant tanks. It has not been considered a practical solution to stabilize sloshing with the control system.[6]

Stabilization of the Saturn vehicles with respect to bending and torsion modes is achieved by shaping networks in each of the control sensor channels. The complexity of the shaping networks is determined by the frequency spectrum they must filter and by the sensor locations.

The influence of control sensor locations can be observed by referring to Figure 8, which shows the Saturn configuration and the first two bending mode shapes. Two possible locations for the rate gyro are shown, one in the Instrument Unit and the other at the rear of the S-IVB stage. One apparent advantage of the S-IVB location is that the slope of the first bending mode is less than it is for the sensor located in the Instrument Unit. In addition, the first and second bending modes have the same slope which would allow phase stabilizing of both modes.

Although more complex networks are required, the rate gyro is located in the Instrument Unit of the Saturn-Apollo because of the improved environment, increased reliability, and reduced cabling and interface problems. Should future Saturn configurations have significantly different bending mode characteristics because of various payloads, the backup location (S-IVB) may be necessary.

The attitude information is derived from the inertial platform which is located in the Instrument Unit. Since the

Table 3. Saturn V Control Gains

First Stage Propulsion Period		
t (seconds)	a_o (deg/deg)	a_1 (deg/deg s^{-1})
0 - 105	0.9	0.69
105 - 130	0.45	0.44
130 - cutoff	0.32	0.30
Second Stage Propulsion Period		
t (seconds)	a_o (deg/deg)	a_1 (deg/deg s^{-1})
0 - 60	1.12	1.9
60 - 190	0.65	1.1
190 - cutoff	0.44	0.74
Third Stage Propulsion Period		
t (seconds)	a_o (deg/deg)	a_1 (deg/deg s^{-1})
0 - 260*	0.81	0.97
260 - cutoff	0.81	0.70

*Throughout S-IVB first burn and to 260 seconds of second burn.

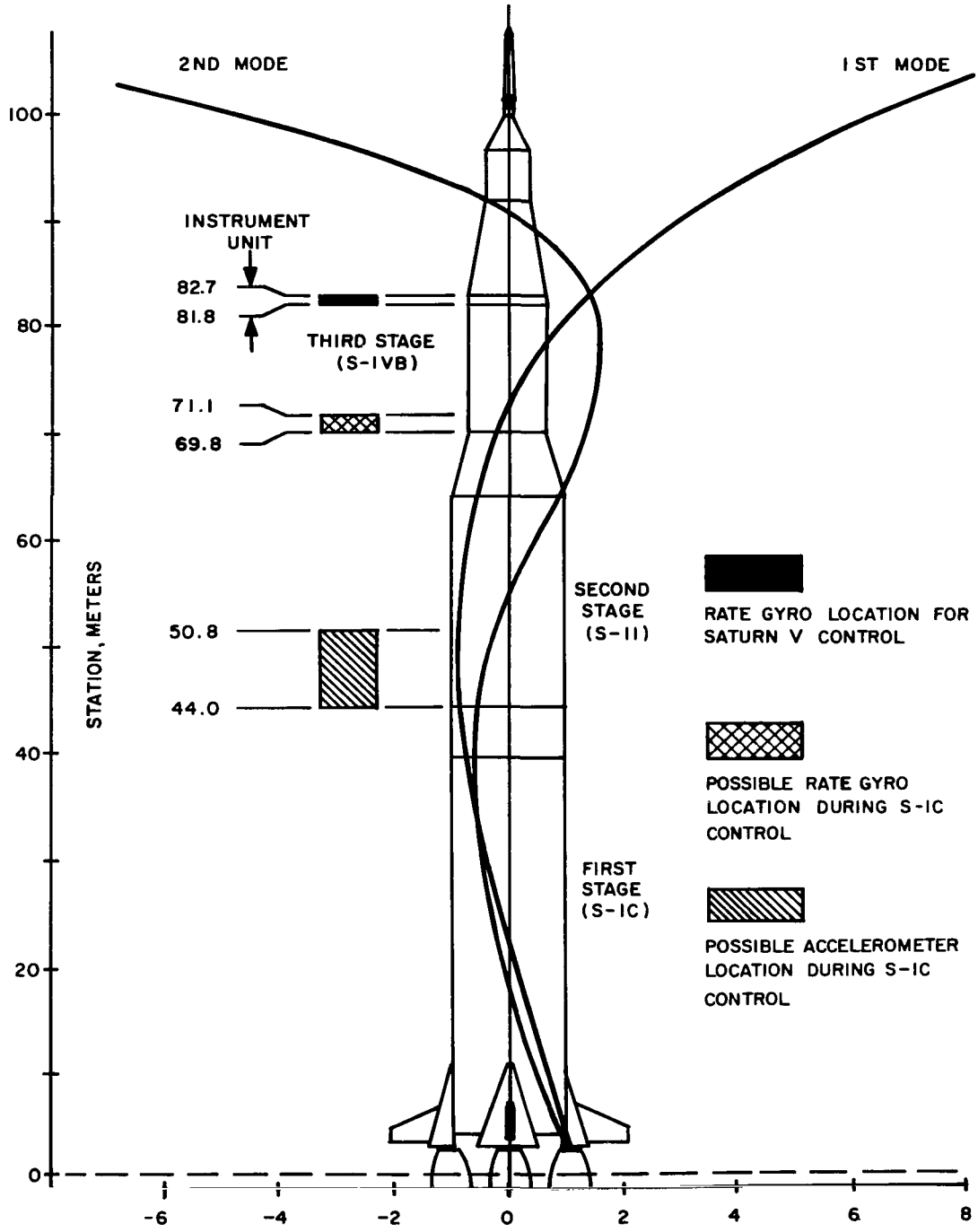

FIGURE 8. SHAPE OF THE FIRST AND SECOND BENDING MODES.

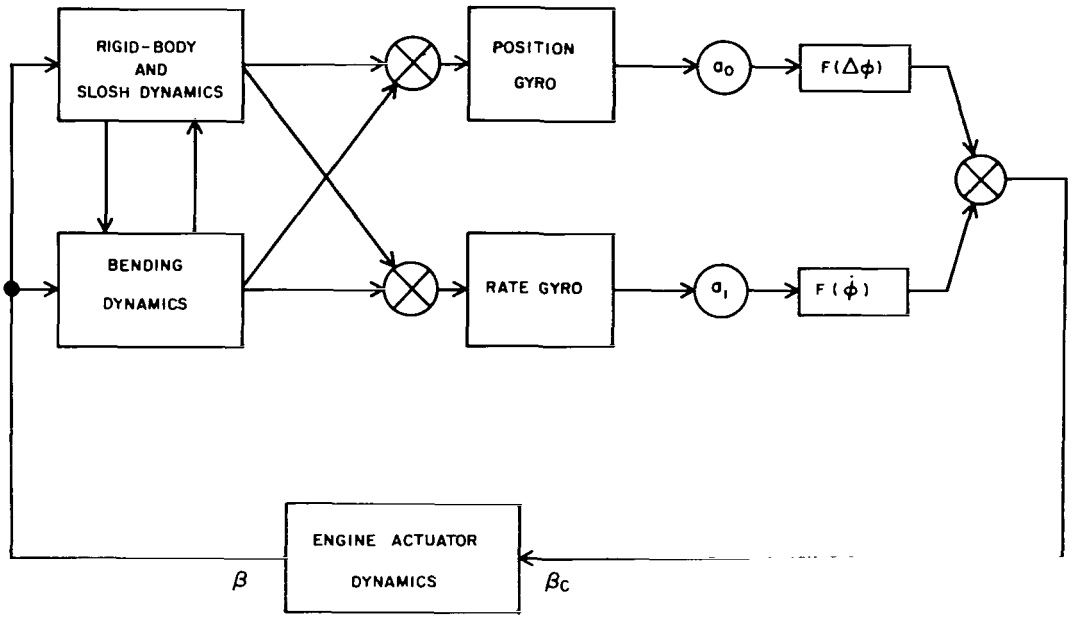

FIGURE 9. BLOCK DIAGRAM OF THE CONTROL LOOPS.

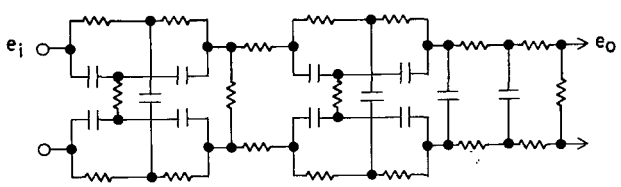

$$\frac{e_o}{e_i} = \frac{G\,[p^2+3.6\,p+430][p^2+0.67\,p+100]}{[p+2.9][p+5.8][p+12][p+56][p+67]}$$

PITCH-YAW ATTITUDE RATE CHANNELS

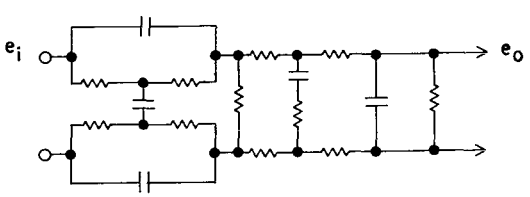

$$\frac{e_o}{e_i} = \frac{G\,[p+0.1]\,[p^2+12\,p+197]}{[p+0.047]\,[p+11]\,[p+30]\,[p+52]}$$

PITCH-YAW ATTITUDE CHANNELS

FIGURE 10. SHAPING NETWORKS

control loop gain at the bending mode frequencies is much less through the attitude loop than through the rate loop, the location of the attitude gyro is not as sensitive and therefore is determined by the need to have one centrally located unit for all stages. The simplified block diagram shown in Figure 9 illustrates the basic control loops for one vehicle axis. $F(\Delta\phi)$ and $F(\dot{\phi})$ are the shaping networks necessary to stabilize the vehicle; a_0 and a_1 are the control gains discussed earlier. Figure 10 shows typical Saturn networks and their transfer functions.

SATURN LAUNCH VEHICLE HARDWARE DESCRIPTION

Overall System and Signal Flow

Figure 11 exhibits the flow of signals and the main components of the guidance and control system. Vehicle attitude and acceleration are measured by the inertial platform and its accelerometers, converted to digital form by the data adapter, and processed by the digital guidance computer.

According to the preprogramed guidance equations, the guidance computer determines cutoff time and control command signals, which are converted from digital to analog in the data adapter. Timed signals and cutoff are processed to the digital switch selectors in the various

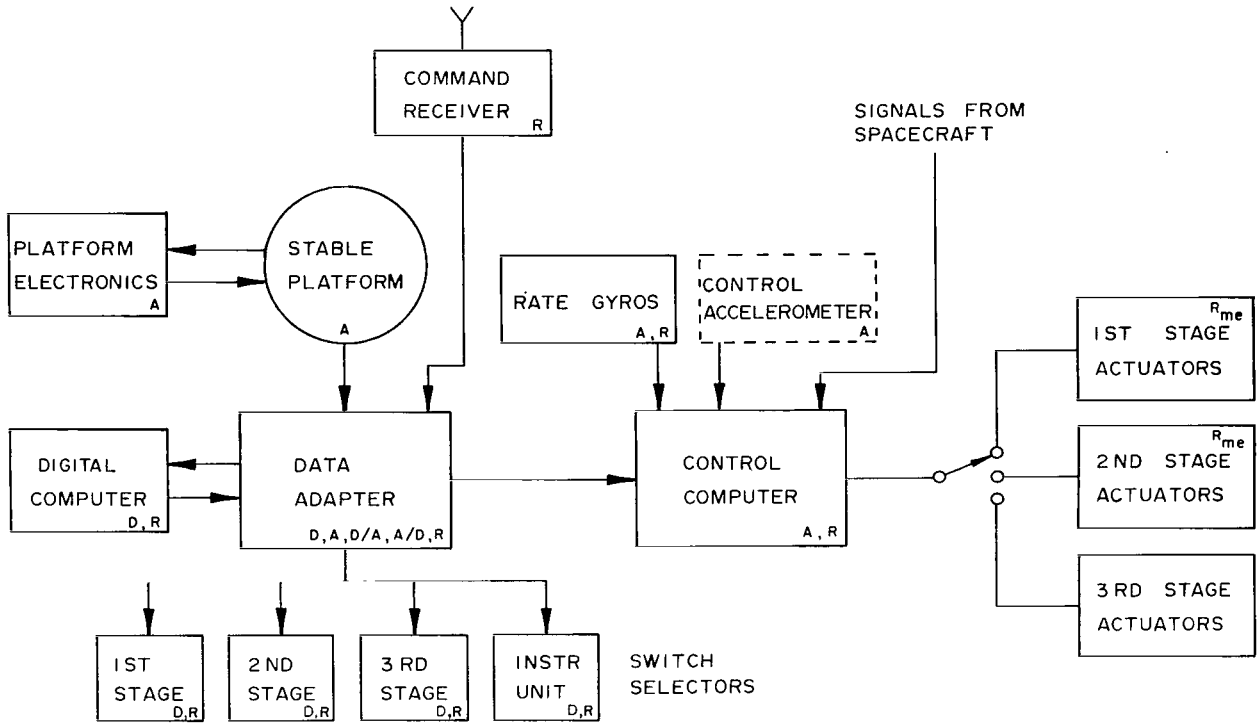

A ANALOG COMPONENTS
D DIGITAL COMPONENTS
A/D ANALOG-TO-DIGITAL CONVERSION
D/A DIGITAL-TO-ANALOG CONVERSION
R REDUNDANCY APPLIED
R_{me} REDUNDANCY BY MULTIPLE ENGINE CONTROL

FIGURE 11. GUIDANCE AND CONTROL FLOW DIAGRAM.

vehicle stages. The data adapter can also accept signals from the command receiver to select alternate guidance and control modes and to update information.

The analog control computer shapes, mixes, and amplifies the guidance and attitude control signals from the data adapter and the damping signals from the rate gyros. If necessary, control accelerometer information can be added to these signals. Alternate guidance and control commands, if needed for backup, can be taken from the spacecraft instrumentation or from manual control. The summed command signals are furnished to the actuators of the various vehicle stages.

The following sections describe in detail the major items of equipment performing guidance and control.

Stable Platform[7]

The ST124-M inertial platform system provides the integrated acceleration data, inertial reference coordinates, and vehicle attitude measurements with respect to these coordinates for guidance and control of the Saturn launch vehicle. The stable platform (Fig. 12) is a three gimbal platform. The inner gimbal is stabilized by three mutually perpendicular single-degree-of-freedom gas bearing gyros mounted on the inner gimbal with their input axes aligned along an orthogonal coordinate system X, Y, and Z. The output axes of the gyros have been oriented with respect to the main thrust vector for minimum error contributions by anisoelastic effects. The inner gimbal further carries three gas bearing pendulous integrating gyro accelerometers with their input axes aligned along

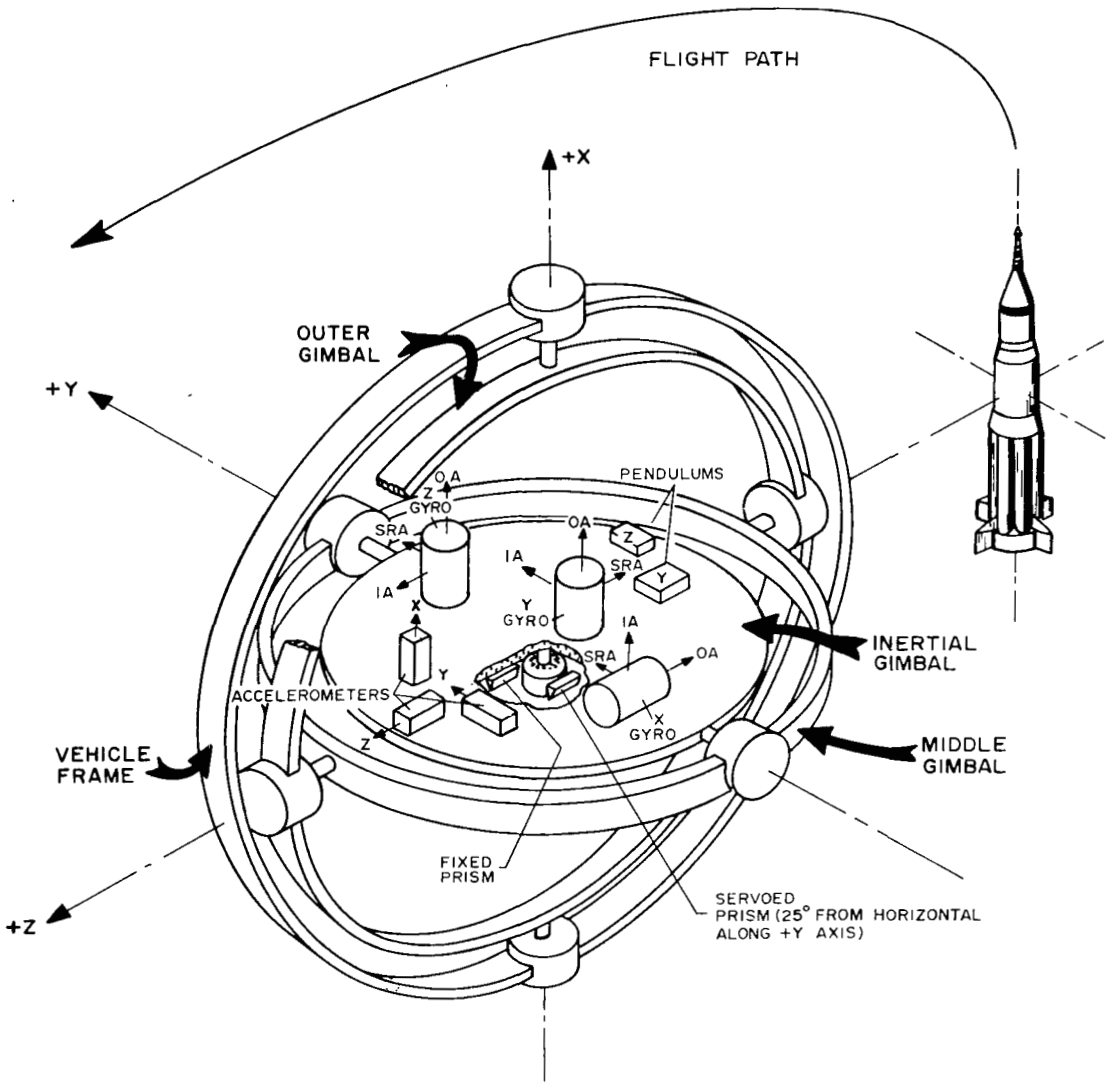

FIGURE 12. STABLE PLATFORM.

the orthogonal coordinate system X, Y, and Z. The measuring head of each accelerometer contains a pendulous single-degree-of-freedom gyro; the position of the measuring head relative to the stable frame is a measure of integrated acceleration along the input axis of each accelerometer.

The platform orientation system will align the X vector along the launch local vertical; the X vector points outward from the earth's surface. The laying system will position the inner gimbal in azimuth so that the Z vector will point in flight direction and the plane formed by the X, Z axes will be parallel to the desired flight plane.

The Y accelerometer that measures perpendicular to the flight plane will provide crossrange guidance. The X and Z accelerometer information will be used to obtain the pitch attitude of the vehicle acceleration vector and the required cutoff velocity.

Figure 13 shows a block diagram of the platform gimbal servoloops. The servoloops use a 4.8 kHz amplitude-

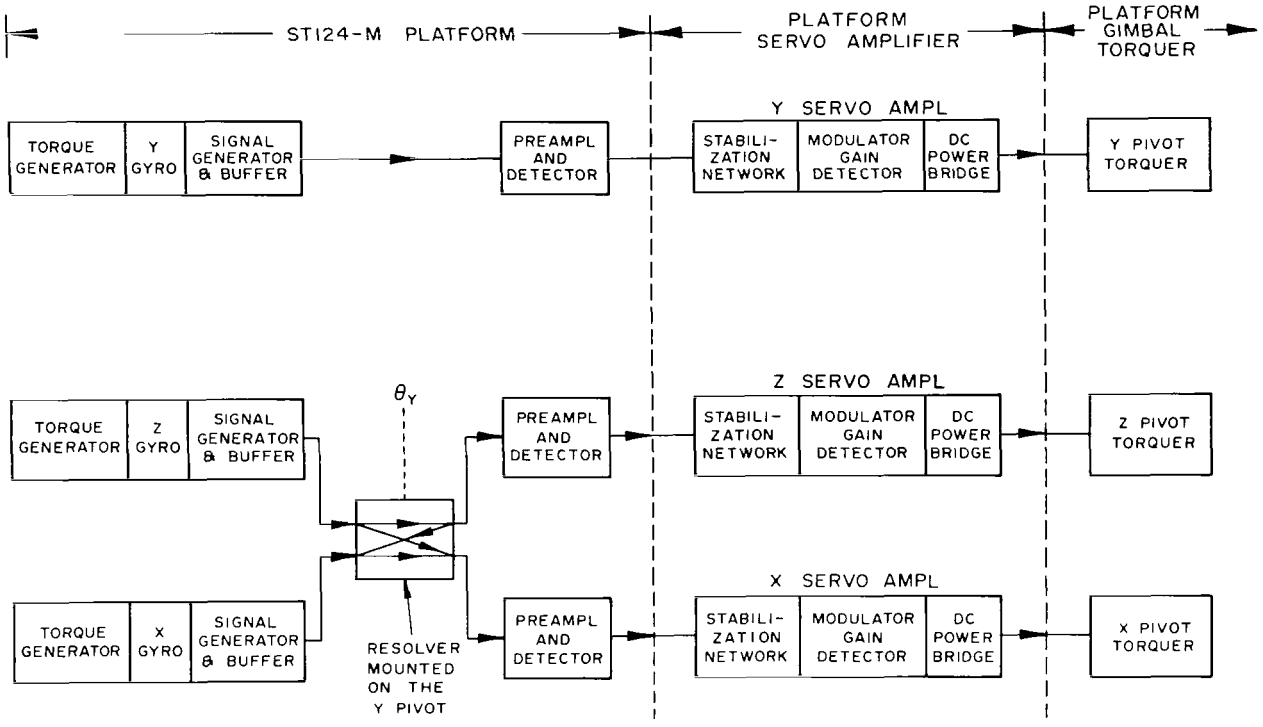

FIGURE 13. GIMBAL SERVOLOOPS.

modulated carrier system with the gyro outputs amplified and demodulated on the gimbals of the platform. The dc signal is shaped in a stabilization network, remodulated at 4.8 kHz, amplified, and then demodulated prior to entering the dc power bridge. This dc power bridge provides a current source drive for the direct axis dc gimbal torquer to obtain a servoloop independent of torquer heating and commutator brush resistance. The 4.8 kHz carrier was chosen to provide sufficient bandwidth for the servoloop.

The Y servoloop has the Y gyro output signal phase-shaped and amplified in the servoamplifier and sent to the Y pivot torquer (the innermost pivot of the platform) as shown in Figure 13. The X and Z gyro output signals are resolved along the X and Z coordinates of the middle gimbal by a resolver mounted along the Y or inner pivot. These outputs of the resolver are preamplified and demodulated on the middle gimbal. The signal to the Z servoamplifier is further amplified and fed to the Z or middle pivot torque generator while the X servoamplifier drives the X or outer pivot torquer. No gain compensation such as secant θ_Z is used in the X servoloop for middle gimbal angles which are $-45° < \theta_Z < 45°$.

The servoloop signals to and from the platform are dc signals and are at a level high enough to neglect slipring noise and resistance variations. Using dc transmission eliminates pickup and cable problems.

Analog resolvers are used for angular readouts; the phase shifts of their output voltages are measured by digital techniques. This method has been preferred to direct digital readout, for which the present technology is not considered to be sufficiently advanced with respect to accuracy and size.

For the demanded high readout accuracy, dual resolvers are used. They possess two independent two-phase windings in the same magnetic structure, one for one-pole-pair and one for multiple-pole pairs.

Prior to launch, the stable platform must be oriented into the measuring directions of the accelerometers with an accuracy of ±20 arc seconds. This orientation is carried out with respect to the local vertical by direct-measuring accelerometers in the form of gas bearing supported pendulums. For azimuth alignment, the inner gimbal contains a fixed prism and a servo-driven prism (Fig. 12). The fixed prism has its porro edge parallel to the X axis while the porro edge of the movable prism rotates in the horizontal plane. The movable prism is driven by a geared servomotor mounted to the inner gimbal through a gear train of 10^5:1, and the angle between the prism and the inner gimbal is measured by a dual-speed control transmitter synchro. The movable prism is continuously servo-oriented to the azimuth reference line of sight. After an initial calibration of the synchro transmitter output when both prisms are pointed in the reference direction, the angle between both prisms corresponds to the necessary rotation angle to orient the Z axis in the flight path azimuth.

Gas Bearing Gyro[8]

The cylindrical externally-pressurized gas bearing provides an almost torque-free support for the output axis of the single-degree-of-freedom gyro. An obvious advantage of this support is that the weight and therefore the angular momentum of a certain size gyro are not limited by average density requirements for the float as in the case of the liquid flotation bearing. Consequently,

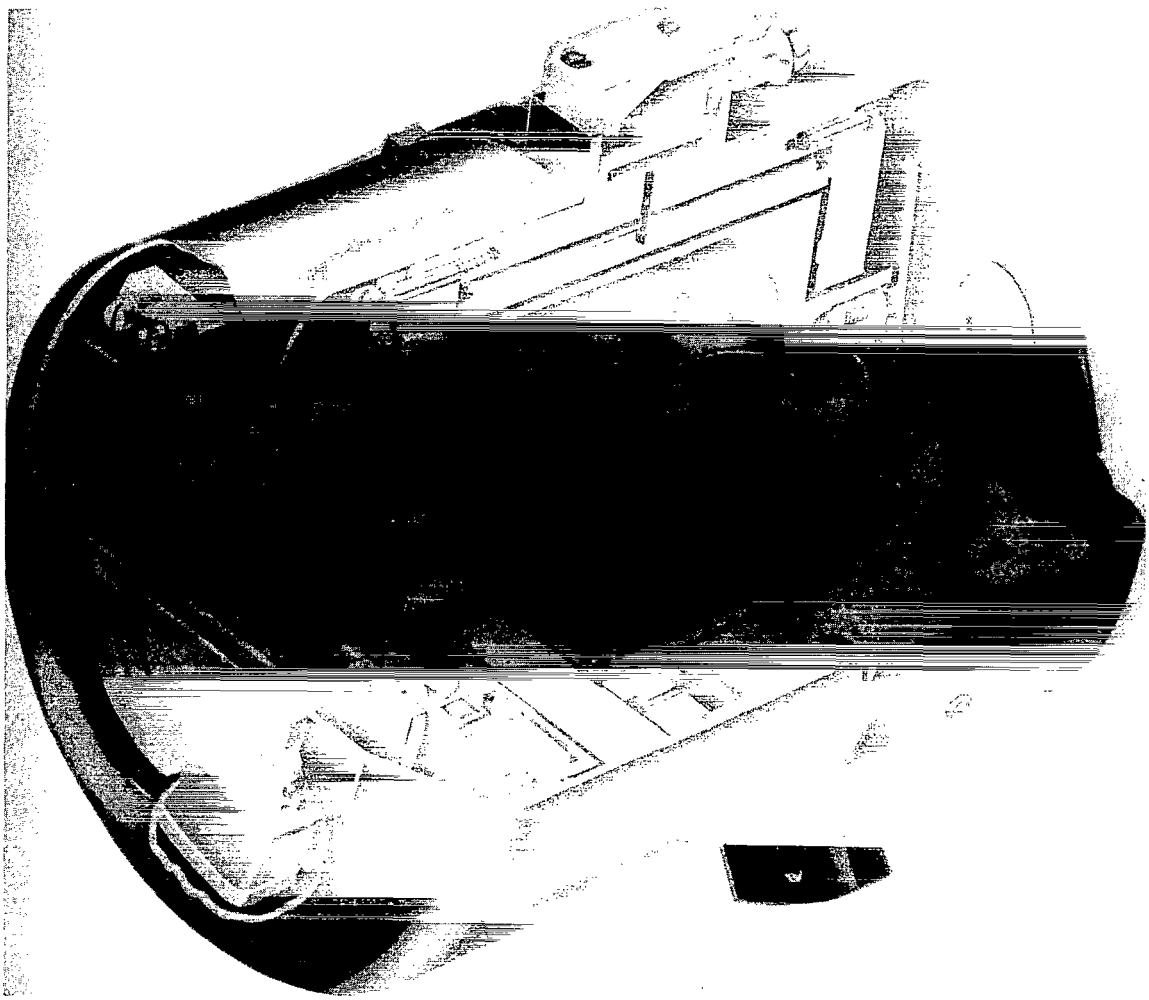

FIGURE 14. GAS BEARING GYRO

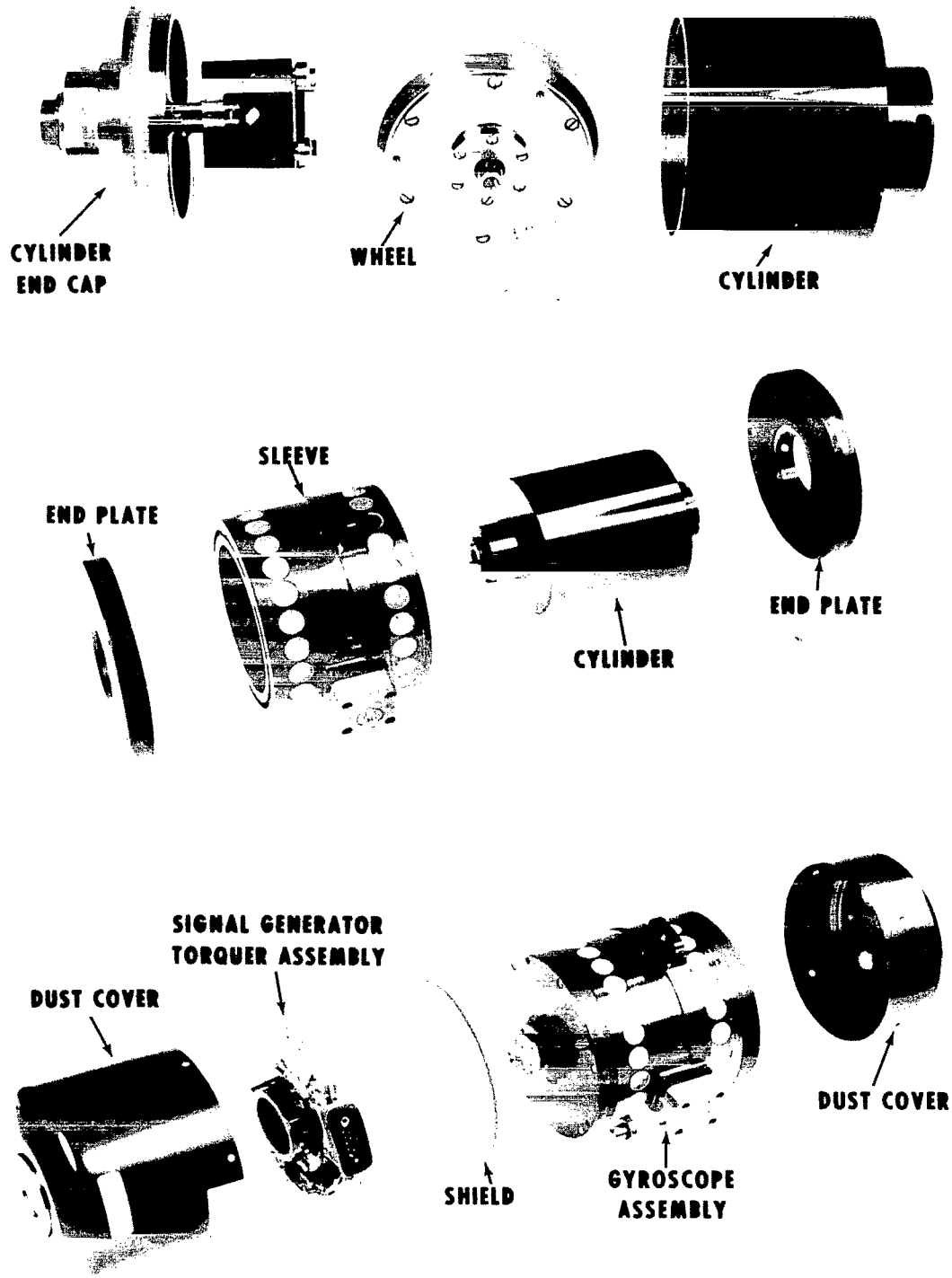

FIGURE 15. GAS BEARING ASSEMBLY

maximum angular momentum with respect to gyro size and high structural stiffness can be obtained; for specified accuracy, comparatively high perturbation torques are possible. Furthermore, modest temperature limits can be imposed to obtain constant accuracy; no need exists to compensate or recalibrate for bias torques.

The gas bearing gyro (type AB5-K8) is shown in a cutaway view in Figure 14. Details of the gas bearing assembly are displayed in Figure 15. Pressurized dry nitrogen gas enters the gap between the cylinder (which contains the gyro motor and flywheel) and the sleeve through two rows of millipore discs, which act as flow restrictors and provide the bearing stiffness. The gas flows symmetrically to both end plates and then escapes around the center openings of these endplates. Thus the cylinder is supported in radial and axial directions.

The signal and the torque generators are of the ac type to avoid magnetic remanent torques, which could occur from dc excitation. The signal generator is a shorted single winding sensor for the angular displacement of the gyro about its output axis. The torque generator operates like an eddy current motor and provides only alignment torques for initial erection.

Some gyro characteristics are shown in Table 4.

Table 4. Characteristic Data of the Gyro and Accelerometer.

Item	Dimension	Gyro	Accelerometer
Gyro Wheel			
Type		synchronous hysteresis	synchronous hysteresis
Angular momentum	[cm^2 g s^{-1}]	2 x 10^6	1 x 10^5
Wheel speed	[rpm]	24,000	12,000
Wheel power at 26 V, 3 phase 400 Hz	[W]	8	4.5
Gas Bearing			
Gas pressure	[N cm^{-2}]	10	10
Gas flow rate	[cm^3/min]	2000	2400
Air gap	[cm]	0.0015 to 0.002	0.0015 to 0.002
Sleeve, end plate, and cylinder material		anodized beryllium	anodized beryllium (end plate Monel)
Signal Generator			
Type		2 pole shorted turn reluctance	4 pole shorted turn reluctance
Excitation (4.8 kHz)	[V]	10	10
Sensitivity	[mV/deg]	550 with 10 kΩ load	285 with 10 kΩ load
Float freedom	[deg]	±3	±6
Torquer			
Type		shorted turn reluctance	direct axis dc torquer
Normal erection rate	[deg/min]	6	
Maximum torque	[N m]		0.±4
Physical Characteristics			
Size	[in.]	3 dia. by 4 length	3.25 dia. by 5 length
Mass	[g]	900	±200
Velocity Pickoff - Optical Encoder (redundant output)			
Scaling	[m s^{-1} rev^{-1}]		300
Resolution	[m s^{-1}/bit]		0.05

Pendulous Integrating Gyro Accelerometer with Gas Bearing[8] (Fig. 16)

The gyro motor and flywheel of the gyro accelerometer are shifted along the spin reference axis to obtain the desired pendulosity about the gyro output axis. The gas bearing containing the gyro is mounted to rotate freely about the gyro input axis, which points in the measuring direction. A signal generator measures angular deflections of the gyro about the output axis and controls the servomotor on the gyro input axis. The precession angle is read out with high accuracy by an optical encoder with redundant readout.

A constant accelerometer scale factor, defined as velocity increment per revolution about the input axis, is guaranteed by a synchronous spin motor supplied from a power source with crystal-controlled frequency. To reduce temperature dependency of the scale factor, mechanical temperature compensation is applied. The increase in pendulosity caused by temperature is balanced by the change in angular momentum of the gyro flywheel which expands with increasing temperature.

Table 4 shows some characteristic data of the pendulous integrating gyro accelerometer.

Digital Computer and Data Adapter

Functions

The digital computer and the data adapter fulfill the computational and input/output requirements for the Saturn launch vehicles. These units, which represent one of the first applications of redundancy techniques in a large scale to operational hardware, also assist in the ground

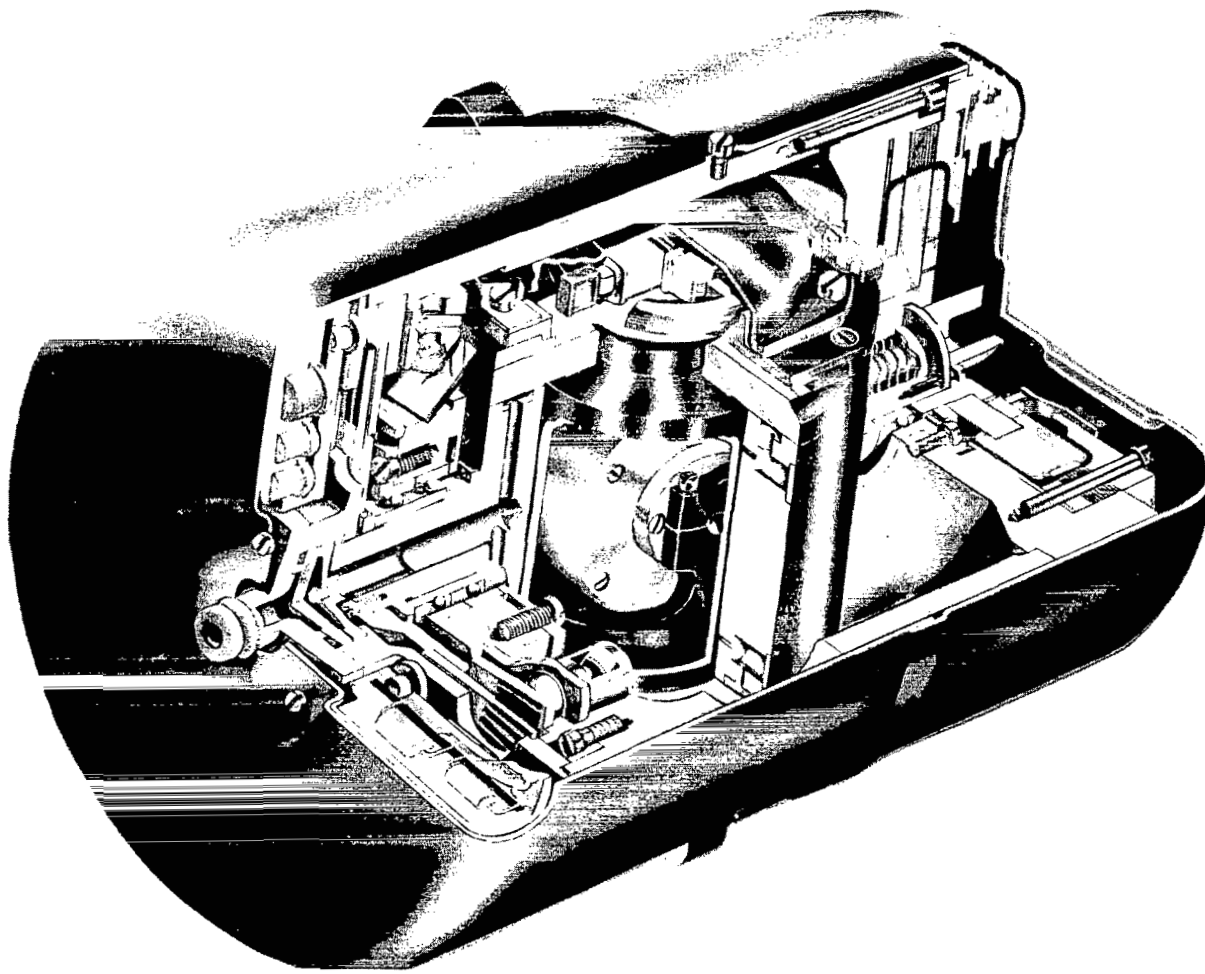

FIGURE 16. PENDULOUS INTEGRATING GYRO ACCELEROMETER.

and orbital checkout of the booster and spacecraft. The operational phases of the system may be considered in the following sequence: prelaunch checkout, launch vehicle guidance, orbital checkout, and translunar injection.

During prelaunch checkout[9], the astrionic system is checked automatically through command from the ground launch computer. The onboard digital computer and data adapter system, in conjunction with the ground launch computer, is utilized to check itself as well as to assist in the checkout of other subsystems in the Instrument Unit (IU), such as the platform accelerometers and gimbal angles, the vehicle switch selector, and the radio command receiver. Furthermore, any measurement normally telemetered from the IU or the third stage can be monitored through the computer. Before launch, all communications between onboard and ground support equipment are handled through the ground launch computer and/or the telemetry system. The ground launch computer sends test variables to the airborne computer, which performs test operations as required from the information and sends the results back to the ground launch computer via telemetry for verification. Guidance constants are loaded in and read back for verification. Test programs are contained in the computer for each mode, and a sequence simulating the actual mission is carried out to check parts of each program.

The computer performs the calculations for navigation and guidance required for the launch vehicle. During the major computation cycle (navigation and guidance loop), the instantaneous position and the velocity vector are determined, and the required velocity direction is computed according to the path adaptive scheme. The gravitational acceleration is computed and combined with the measured velocity, and coordinate resolution utilizing platform gimbal angles is accomplished. These computations have a repetition time of approximately two seconds. In the attitude correction or minor computation loop, steering commands are computed and sent to the attitude control system at a rate of approximately 25 times per second (Fig. 17).

In earth orbit, the digital computer checks out the IU as well as the propulsion, attitude control, radio command, guidance, and telemetry subsystems. The computer and data adapter sequentially initiate stimuli to each system and compare the telemetry data with prestored go/no-go

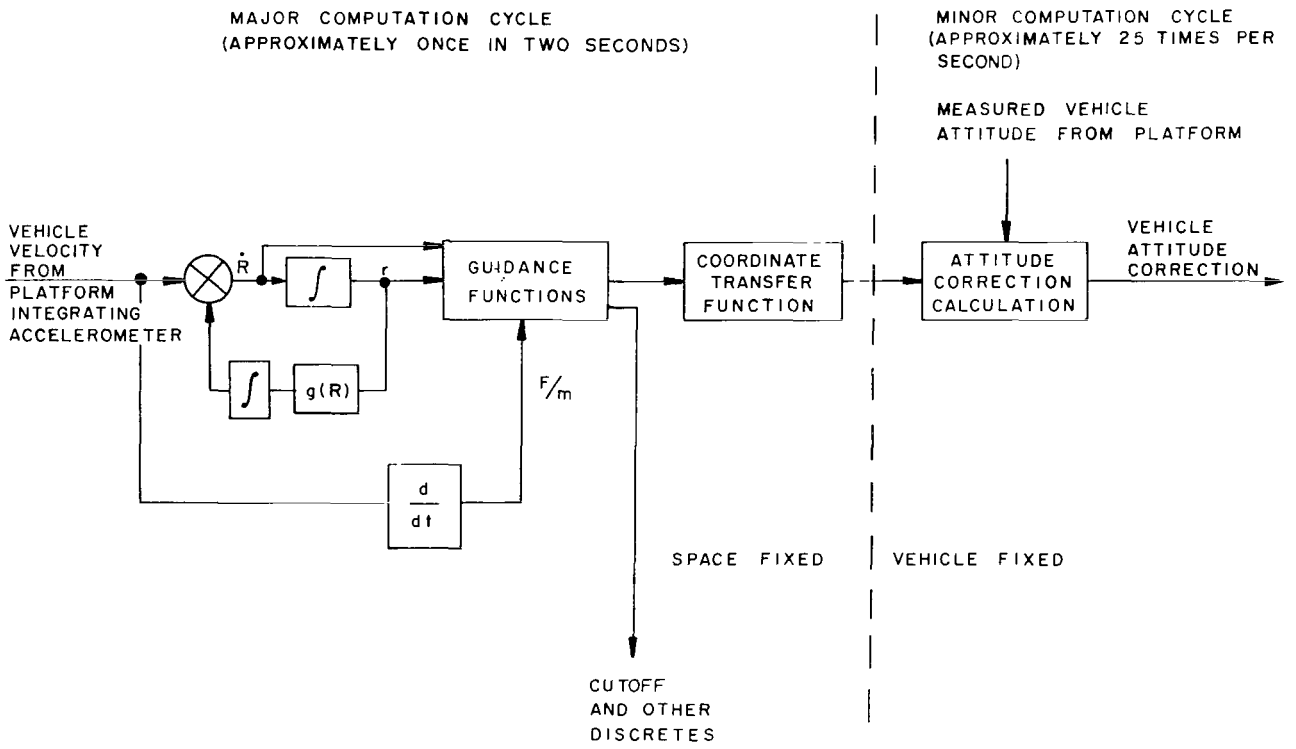

FIGURE 17. MAJOR AND MINOR COMPUTATION LOOPS.

values. Any IU or third stage measurement that is telemetered can be read by the computer and data adapter. Data and control information necessary for checkout may be inserted into the computer from the ground via the radio command link.

The computations required for translunar injection are similar to those used for guidance into earth orbit.

The data adapter interconnects the digital computer, the main guidance and control components, the switch selectors, the telemetry system, the power supplies, the ground launch computer, and the peripheral IU equipment; digital-to-analog and analog-to-digital conversion is included in this interconnection assignment.

The computer system utilizes microminiature packaging techniques as far as feasible. Semiconductor chips are mounted on square ceramic wafers (side length 7.5 mm) on which interconnecting wiring and film resistors have been deposited by silk screen printing and firing. The devices, called unit logic devices, are soldered to multilayer interconnection boards. Each multilayer interconnection board has a capacity of 35 unit logic devices. Two multilayer interconnection boards are bonded back-to-back to a supporting metal frame to form a logic page assembly. Multilayer interconnection boards and pages are joined by connectors to a central multilayer printed circuit board (Figs. 18 and 19).

For applications requiring extreme accuracy or large drive current capability, circuit modules composed of conventional discrete components are utilized. These find greatest application in the data adapter but are also used in the computer as memory drivers.

The magnesium-lithium frames of the digital computer and the data adapter are liquid-cooled to remove heat generated by the electronic components. This cooling results in a low operating temperature for the electronic components and thus in a high reliability for the devices.

The use of various redundancy techniques for further improvement of the reliability considerably increases the number of electronic components in a system.[10] In the case of triple modular redundancy, approximately 3.4 times as many components are required as in a simplex system. However, with the application of redundant logic, several failures are possible without a system failure. Thus, despite the increase of component failures with the number of components, a triple modular redundant system is more reliable than a simplex system by a factor of approximately $(3R-2R^2)^N$, where R is the reliability of a module and N is the number of modules in a simplex machine. To guarantee effective triple modular redundancy before launch, component failures will be reported by disagreement detectors and the modules concerned will be replaced by the plug-in page assemblies shown in Figure 19.

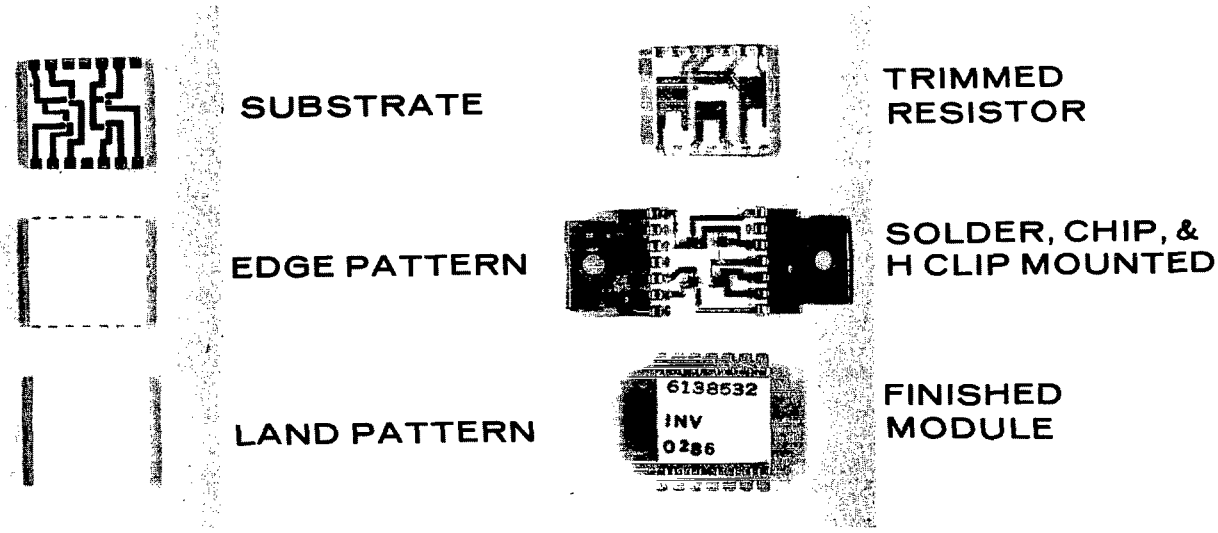

FIGURE 18. UNIT LOGIC DEVICE BUILDUP (ACTUAL SIZE).

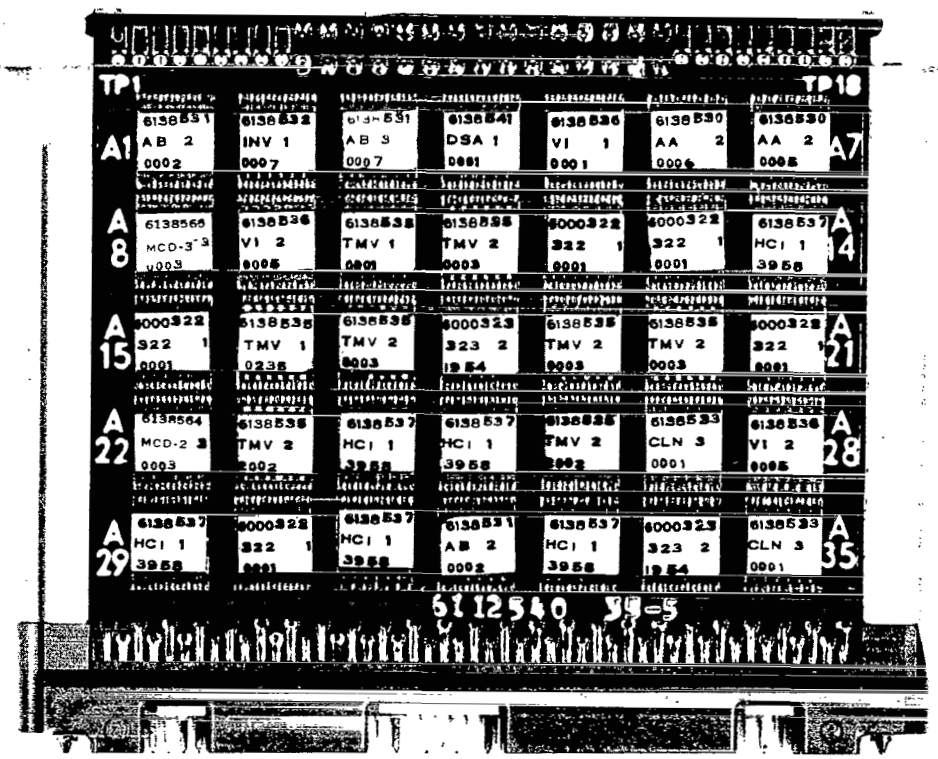

FIGURE 19. MULTILAYER INTERCONNECTION BOARD.

Self-testing features and reasonableness checks are programed into the computer system. Thus input signals and their conversion into digital information are evaluated, such as the angular readout of the stabilized platform gimbal resolvers, the accelerometer velocity increment readout, and angular vehicle rates. The logic process may demand comparison of fine and coarse readout of signals, comparison of redundant evaluation, comparison with programed standard values, change and selection of signals, and replacing unacceptable information by prestored data or by earlier correct values. This logic procedure does not correct or identify the error source, but it prevents gross errors from causing corresponding large errors in the navigation, guidance, and control quantities.

As an example, the accelerometer signal evaluation is described. The optical encoder of the accelerometer provides redundant (A and B) readout in the form of pulses. These pulses (each representing 0.05 m/s) are accumulated in the delay lines in the data adapter. The contents of the delay lines must be read at the beginning of each computation cycle to obtain the velocity data words, each of which contains the redundant optisyn pulse counts in the following bit configuration: AAAAAAAAAAAASSBBBBBBBBBBBB, where A represents the A-optisyn reading, B represents the B-optisyn reading, and S represents spare bits. The A and B readings must be separated, and the differences between the current and past values for each reading must be computed. The resulting differences, ΔA and ΔB, represent the measured velocity changes during the last computation cycle.

If the measured changes, ΔA and ΔB, for each axis agree within two pulses (0.1 m/s), ΔA will be used for the zero and reasonableness tests. If they differ by more than two pulses, the velocity change closer to the expected change must be used for the zero and reasonableness tests. The expected velocity data change used for these tests is obtained by resolving through the measured gimbal angles from the total acceleration (or its preset value during periods of erratic performance) obtained from the previous computation cycle and its time duration.

Since an unchanging accelerometer output during boost periods is an identifiable failure mode, the velocity data changes selected by the disagreement test must be zero tested. All changes greater than one pulse are considered nonzero and are tested immediately for reasonableness. If a zero change is unacceptable, it must be replaced by a backup value derived from a prestored acceleration profile. A velocity data change selected by the disagreement and zero test will be judged reasonable if it stays within a certain band of the expected change; this band may include a nonzero tolerance or may provide a wide tolerance during portions of flight when sudden changes in acceleration occur legitimately. If a measured change fails to pass the reasonableness test, it must be replaced by a backup value derived from a prestored acceleration profile.

The following sections describe the computer and data adapter and show how these units are integrated into the launch vehicle guidance and control system.

General description of the digital computer

The digital computer is a serial, fixed-point, stored program, general purpose machine. Special algorithms have been developed and implemented for multiplication and division[11]; multiplication is done four bits at a time and division is done two bits at a time. The machine utilizes random-access magnetic core memory, triple modular redundancy logic for the central computer, and duplex memory modules. Ultrasonic glass delay lines are used as serial arithmetic registers and as dynamic storage for the instruction counter. The delay lines are used similarly to revolvers in a drum machine and provide temporary storage at relatively small weight and volume. Salient characteristics of the computer are summarized in Table 5. Data words of 28 bits (25 magnitude bits, 1 sign bit, and 2 parity bits) are used in computation. The memory is arranged so that one data word or two instructions (each instruction then contains a parity bit) may occupy one 28-bit memory word.

Table 5. Computer Characteristics

Type	Stored program, general purpose. serial, fixed-point, binary
Clock	2.048 MHz clock, 4 clocks per bit, 512 kilobits per second
Speed	Add-subtract and multiply-divide, simultaneously
Add time, accuracy	82 μs, 26 bit
Multiply time, accuracy	328 μs, 24 bit
Mult-hold time, accuracy	410 μs, 24 bit
Divide time, accuracy	656 μs, 24 bit
Memory	Random access toroidal core
Storage Capacity	Up to a maximum of 32,768 28-bit words in 4096 word modules
Word Length	Memory word 28 bits: Two instructions may be stored in 1 memory word
Data	26 bits plus 2 parity bits
Instruction	13 bits plus 1 parity bit
Input/Output	External: computer-programed Input/output control: external interrupt provided
Component Count*	40,800 silicon semiconductors and cermet resistors Up to 917,504 toroidal cores
Reliability*	0.996 probability of success for 250 hours using TMR logic and duplex memory modules
Packaging	Structure constructed oi magnesium-lithium material, designed to house 73 electronic pages and 8 memory modules
Weight [kg]	35 (4 memory modules)
Volume [m^3]	0.07
Power [W]	137.0 (4 memory modules)

*Figures given here are estimated values.

Each memory module consists of fourteen 128 x 64 magnetic core planes plus the required drive and sensing circuits. The basic module contains 4096 nonredundant 28-bit words. For flexibility in memory size, the number of modules may vary from one to eight. With eight memory modules operating in simplex, the computer has a 32,768-word memory capacity, which is equivalent to the basic memory capability of the IBM 7090 commercial machine. The memory modules operate independently, allowing duplexing for higher reliability. Storage external to the memory is located predominantly in the glass delay lines.

The reliability of the computer is predicated on the use of triple modular redundancy in the central computer logic. Figure 20 indicates the organization of the computer from a reliability standpoint. Calculations and simulations based on Monte Carlo techniques indicate a reliability of 0.996 for 250 hours (0.999966 for a 6-hour mission) for the computer logic and memory using triple modular redundant and duplex techniques, respectively. For comparison, the equivalent simplex logic has a reliability figure of 0.955 for 250 hours. Theoretically, the reliability of duplex modules exceeds that of triple redundant modules by a factor $\frac{2R - R^2}{3R^2 - 2R^3}$, but the difference is of a second order effect for values of R close to "one" and therefore negligible. Duplex redundancy, however, has limited application because of the problem of determining which one of the two units failed.

The triple modular redundant logic system uses three identical simplex logic channels and subdivides each channel into seven functional modules. The outputs from corresponding modules are voted upon in voter circuits before the signal is sent to the next modules. Figure 21 shows typical modules and voters. The output of the voter circuit is equal to the majority of the inputs to the circuit. Thus, even if one of the three inputs is incorrect, the output to the next module will be correct. The voter circuit outputs may go to any of the other subdivided modules of the computer. This allows correct computations to be obtained, even with several malfunctions in the computer, provided two modules of a triple redundant set are not in error.

Disagreement detectors are used on module outputs as shown in Figure 21 to indicate a failure in the system. Approximately 13 disagreement detectors are logically combined and fed to a register in the data adapter. The signals are then fed to the telemetry buffer register for monitoring either before launch or in flight.

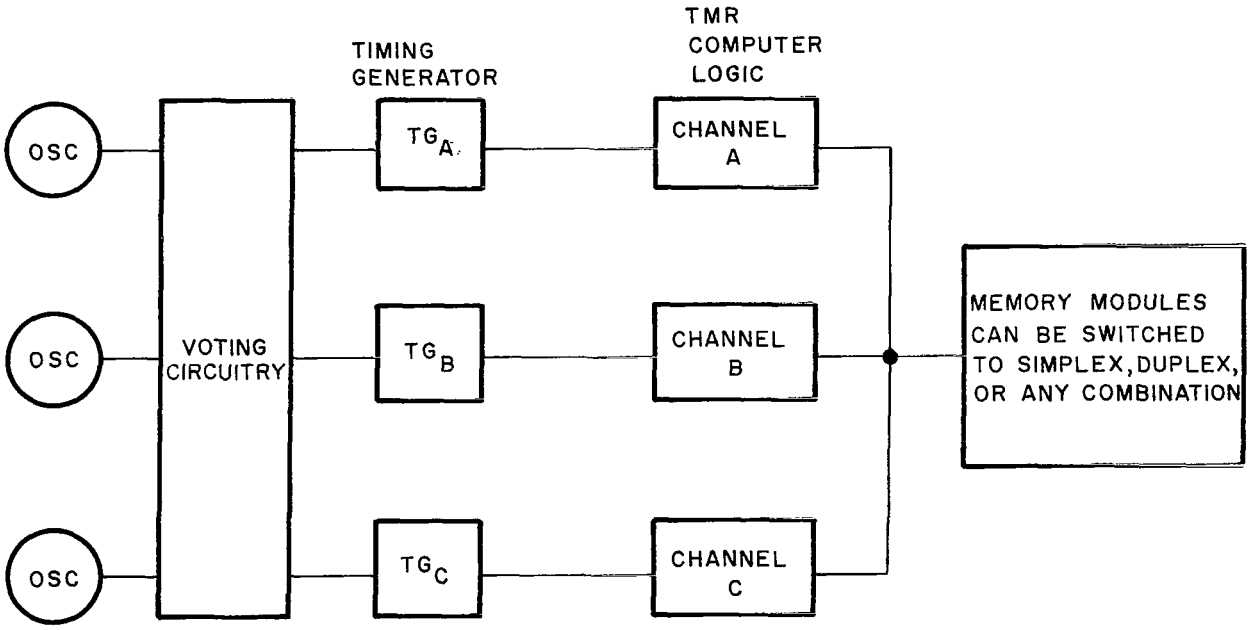

FIGURE 20. COMPUTER REDUNDANCY CONFIGURATION.

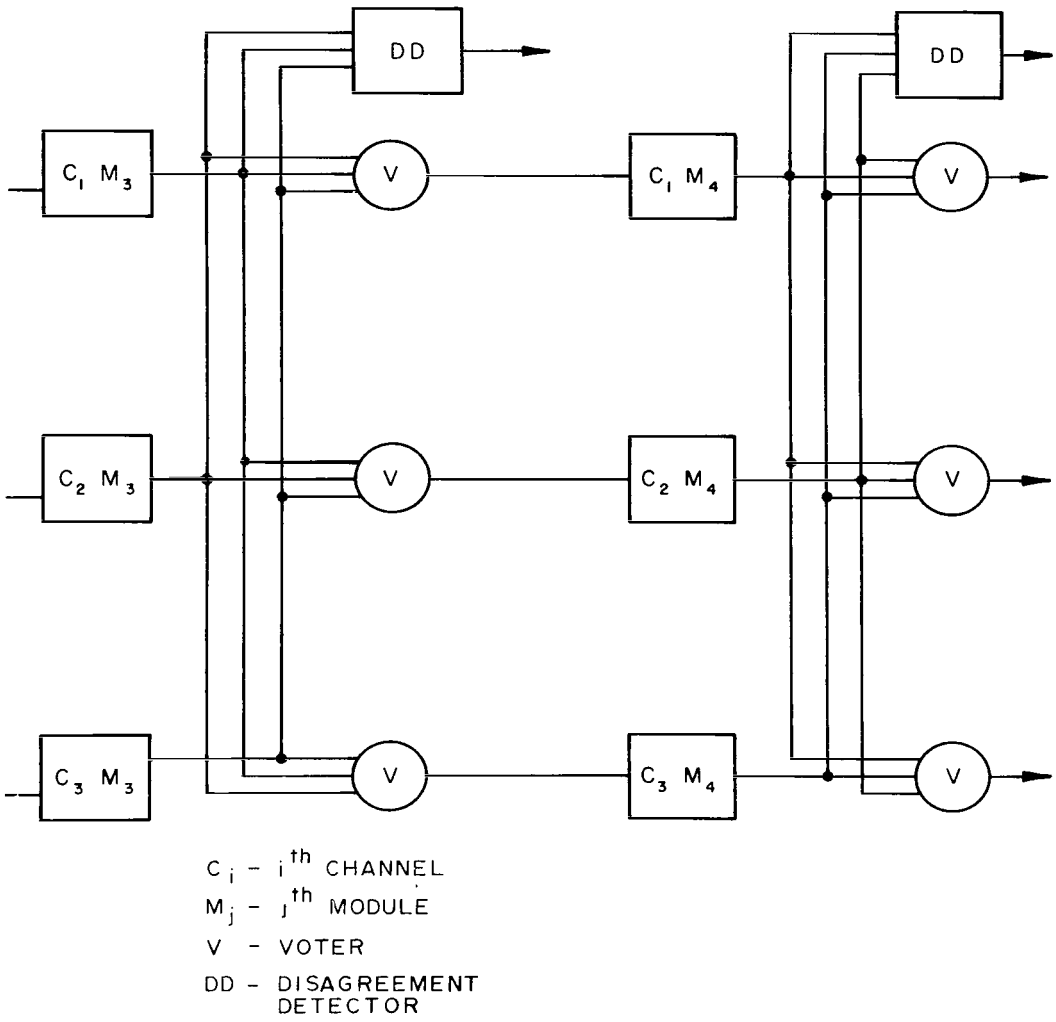

FIGURE 21. TRIPLE MODULAR REDUNDANCY.

General description of the data adapter

The data adapter is the input/output unit for the digital computer and communicates with other launch vehicle equipment and with the ground checkout equipment. The data adapter is capable of transforming input and output signals acceptable to the digital computer and other interconnected equipment. It controls data flow, provides temporary data storage where necessary, and performs certain simple computational and logical operations on data. The functions and interfaces of the data adapter are shown in block diagram form in Figure 22.

The data adapter converts signals in either direction as required to interface digital and analog equipment. In particular, the data adapter supplies data to, and accepts data from, the digital computer at a 512 kHz rate upon command by the digital computer. It accepts and decodes data address signals from the digital computer and provides the digital computer with interrupts and

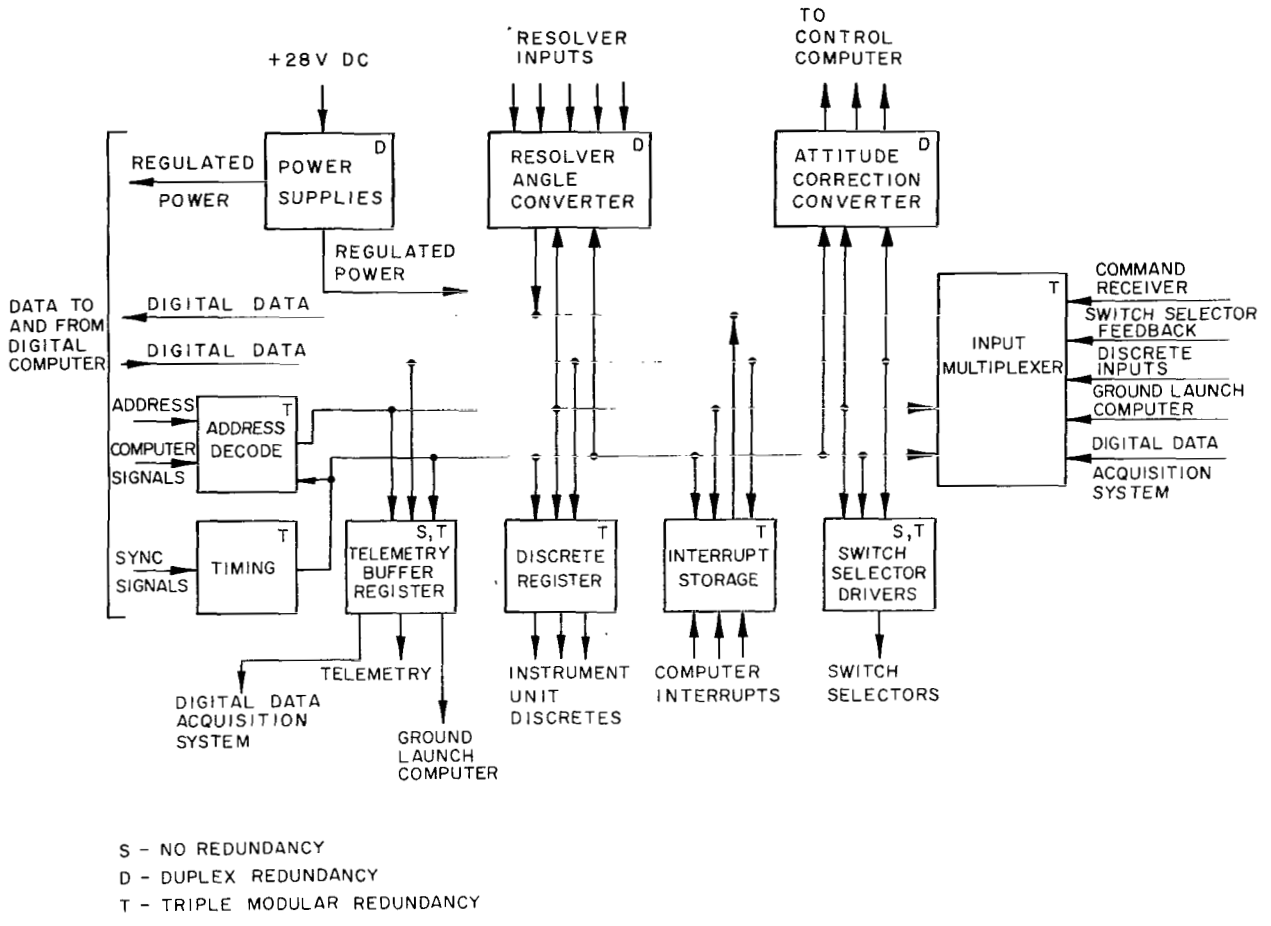

FIGURE 22. DATA ADAPTER/COMPUTER INTERFACE.

miscellaneous control signals. It also accepts synchronizing signals from the digital computer and generates a set of timing signals that is in synchronism with those of the digital computer.

Furthermore, the data adapter provides regulated dc power for its own operation and for the digital computer; it also contains circuitry for channel switching, power supply switching, and sequencing. Data adapter dc power supplies excite the resolvers on the platform with sinusoidal voltage.

A summary of the data adapter characteristics is shown in Table 6.

To improve reliability, various types of redundancy are employed throughout the data adapter. Figure 22 indicates the type of redundancy used in each part. Triple modular redundancy is employed in the flight critical portion of the digital circuitry similar to its application in the digital computer logic.

Power supplies are used in duplex redundancy; isolation diodes allow one amplifier to continue its operation in case of a failure of the other amplifier.

Functional aspects of the computer system

Some of the functional aspects of the computer and data adapter are discussed as well as their integration into the overall vehicle system. The cases considered represent only typical functions.

Table 6. Data Adapter Characteristics

Item	Description
Computer input/output rate	512-kHz serial
Power supplies	6 duplexed regulated dc supplies 2 ac resolver power supplies
Switch selector	8-bit switch-selector input 15-bit switch-selector output
Discretes	7 interrupt inputs from IU 13 discrete outputs 32 discrete inputs
Buffer register Tag register Mode register	26 bits } provides communication with the RCA-110 9 bits } ground control computer, telemetry transmitter, 6 bits } and digital data acquisition system
Digital-to-analog converter	8 bits plus sign, 2-ms operation, 3 attitude commands, and 2 spare outputs
Analog-to-digital converter Platform Spares	Equivalent of 17 bits from a two-speed resolver 4 two-speed gimbal angle resolver inputs 6 single-speed accelerometer resolver inputs 4 single-speed resolver inputs
Delay lines	3 four-channel delay lines for normal operations 1 four-channel delay line for telemetry operations
Telemetry	
Command receiver	14 bits for input data
Data transmitter	38 data and identification bits plus validity bit and parity bit
Digital data acquisition	15 bits address plus validity bit for output data, 10 bits for input data
Input from RCA-110 computer	39 data and identification bits plus validity bit for output data 14 bits for input data plus interrupt
Component count	37,000 silicon semiconductors, cermet resistors, and other special components
Reliability	0.99 probability of success for 250 hours of operation; uses TMR logic, duplex special circuits, duplex power supplies
Packaging	125 electronic page assemblies plus special electronic assemblies
Weight [kg]	86
Volume [m^3]	0.1
Power without computer [W]	400

The primary purpose of the computer system is to issue control commands and flight sequence signals to the vehicle system during flight. These signals can be considered dynamic in nature because they result in vehicle motion or action. Other functions can be considered passive, but nevertheless are of extreme importance; they include the operation of the computer system with the telemetry system, the ground launch computer, and the radio command system. The ground launch computer is used during ground checkout, whereas the radio command system and the telemetering system are operational in ground checkout as well as in flight.

The control commands are evaluated in a major and a minor computation cycle. During the major cycle, which occurs approximately once in two seconds, a solution to

the guidance equation is obtained. The guidance equation is a function of vehicle position ($\bar{R}$), vehicle velocity ($\dot{\bar{R}}$), acceleration (F/m), and real time (t). All parameters, with the exception of real time, are derived from the velocity measurement inputs; time is accumulated in the data adapter. Other operations performed during the major loop are vehicle sequencing for flight events, discrete outputs, telemetry outputs, and miscellaneous control functions within the data adapter.

During the minor loop, the vehicle attitude correction is computed. Attitude correction outputs $\Delta\phi_{x,y,z}$, shown in Figure 23, are dependent upon platform gimbal angles $\theta_{x,y,z}$ and upon the result of the guidance equation calculated in the major loop. The minor loop calculations are made approximately 25 times per second. The attitude correction signals must be updated often enough that the attitude correction change occurring between any two sampling periods is small. These criteria are necessary to prevent the discrete nature of the attitude correction angles from causing any perturbations in the vehicle attitude or causing the vehicle to become unstable.

The digital computer is sequenced through the computation cycles by a set of instructions stored in the computer memory (Fig. 23). If the digital computer is in the

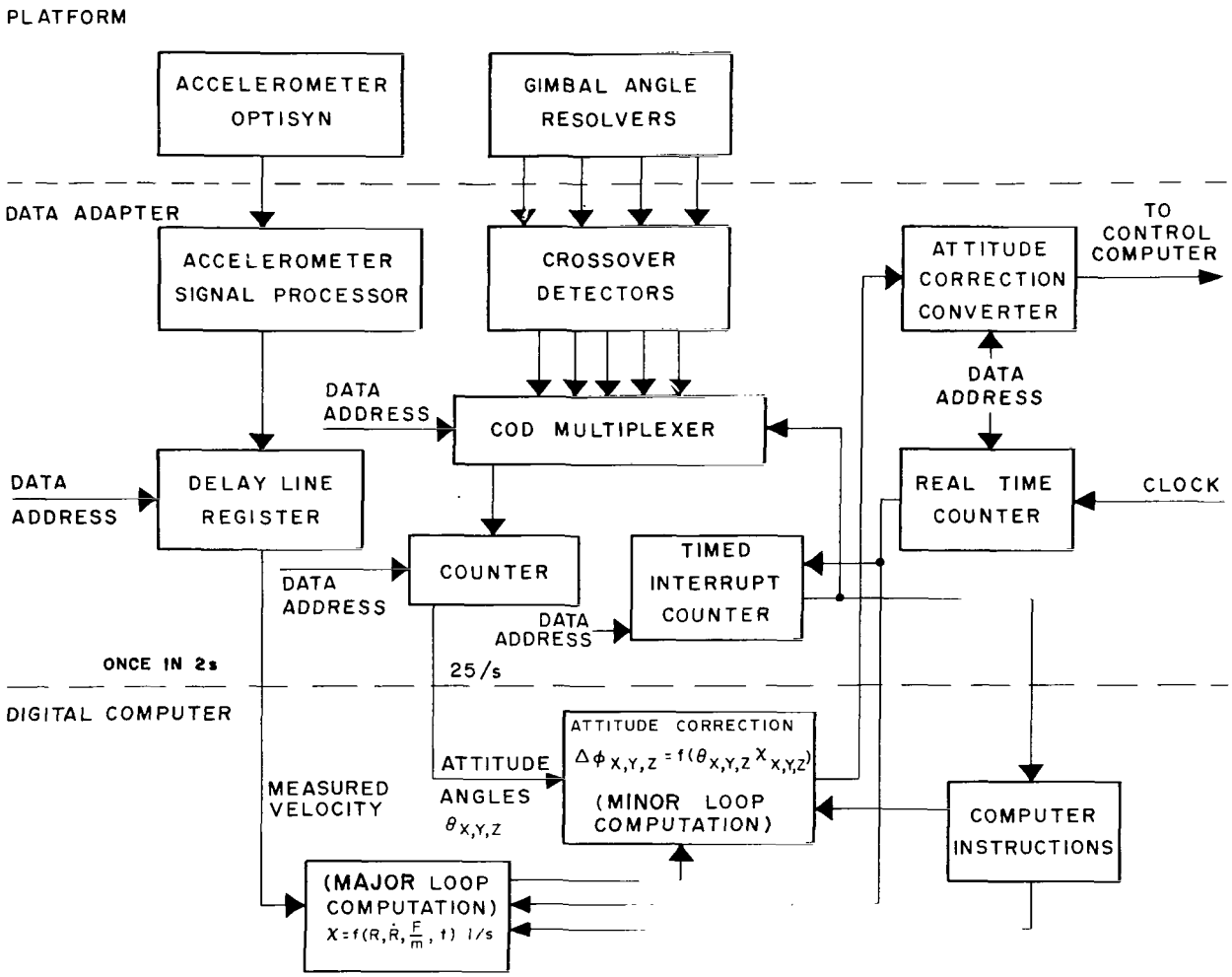

FIGURE 23. NAVIGATION AND GUIDANCE COMPUTATIONS

major computation loop, it will obtain vehicle velocity information from the optical encoders (optisyns) on the accelerometers of the stabilized platform as accumulated in the data adapter. The optisyns generate electrical square-wave signals (gray code) indicating the rotations of the accelerometer shafts. The signals are converted into true binary numbers in the data adapter. The resolution of the converted accelerometer data is 0.05 m/s.

The velocity readings from the platform integrating accelerometers are combined with the gravitational acceleration to yield the velocity components $\dot{X}$, $\dot{Y}$, $\dot{Z}$, which are accumulated in the computer. By time integration of the velocity components, the vehicle position R (X, Y, Z) is computed.

To obtain the thrust acceleration (F/m) required for guidance computations, the velocity readings are differentiated (division of the incremental velocity readings by the time elapsed between two readings). From the resulting acceleration components, the term F/m is computed by taking the square root of the sum of the squares (Fig. 15).

Real time is accumulated in a delay line in the data adapter by counting computer phase times. Whenever the accelerometer optisyns are read, the real time increment in the data adapter is also read. The real time increments are combined in the digital computer with the old values to produce the new values of real time that existed when the accelerometers were read.

The discussed values such as real time, absolute acceleration, vehicle position, and vehicle velocity are used during the major loop computation to calculate the desired gimbal or χ angles. These χ angles are used during the minor loop computations.

During the major computation loop, the digital computer also selects and reads the coarse gimbal angle resolvers located on the stabilized platform. The resolver signals are selected and gated through the multiplexer by energizing a set of data address lines with a digital address.

The computer program enters the minor loop by a signal from the minor loop timed-interrupt counter. The computer stores in the counter a number that is counted down to zero. When it reaches zero, a signal is sent to the digital computer that causes it to switch from major loop computations to minor loop computations.

The signal also selects the first fine gimbal angle resolver and gates the resolver signal through the multiplexer to the counter. By the time the computer processes the interrupt and switches to the minor loop, the first gimbal angle reading is in the counter and is ready for use by the computer. The computer data address that gates the counter reading into the computer also gates the next fine gimbal angle resolver signal through the multiplexer to the counter.

The fine gimbal angle readings are combined in the computer to form the total gimbal angle. This value is compared to the coarse gimbal angle readings as a check against failures. The gimbal angles ($\theta_{X,Y,Z}$) and the extrapolated values of the χ angles ($\chi_{X,Y,Z}$) are used in the minor computation loop to obtain attitude correction angles.

After the attitude correction angles are computed, they are sent to the attitude correction converter in the data adapter, converted to analog signals, and routed to the proper output channel by data address signals from the digital computer.

As previously stated, the rate at which the attitude correction signals are updated is an important factor for vehicle stability. The attitude error angles are updated 25 times per second or every 40 ms. The minor loop program requires approximately 18 ms to read all the fine gimbal angles and compute the attitude correction angles.

After the three attitude-correction angles have been sent to the data adapter, the digital computer enters a number into the minor loop timed-interrupt counter. This number represents the time-to-go to the beginning of the next minor computation loop. After this operation, the computer program returns to the point from which it left the major loop and continues major loop computation until another minor loop interrupt is generated by the minor loop timed-interrupt counter.

Control Computer and Control Sensors[12]

Control computer

During powered flight, the incoming analog signals are filtered and summed with the proper polarity and relative gain factors in the control computer to form individual commands for each hydraulic servoactuator of the engine gimbaling system. Figure 24 shows a diagram of the major elements of the control computer required to form the command of one axis only for one engine servo. Figure 25 shows a functional sketch of the actuator orientations on the different stages. Simultaneous equal commands to the pitch or yaw servos result in net thrust deflections in the pitch or yaw plane. For the first and second stages, roll torques are initiated by simultaneous commands to the pitch and yaw servos. Roll torques are produced from the auxiliary propulsion system during the third stage of flight.

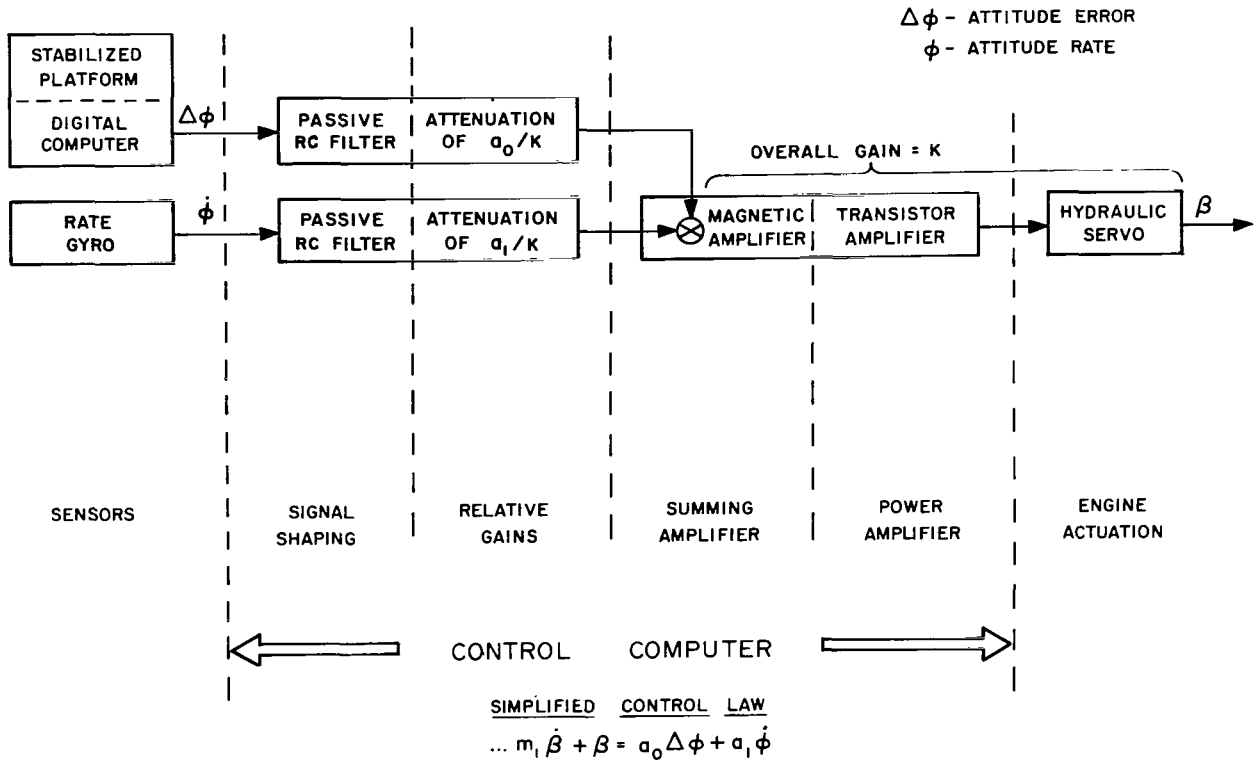

FIGURE 24. ELEMENTS OF THE CONTROL COMPUTER.

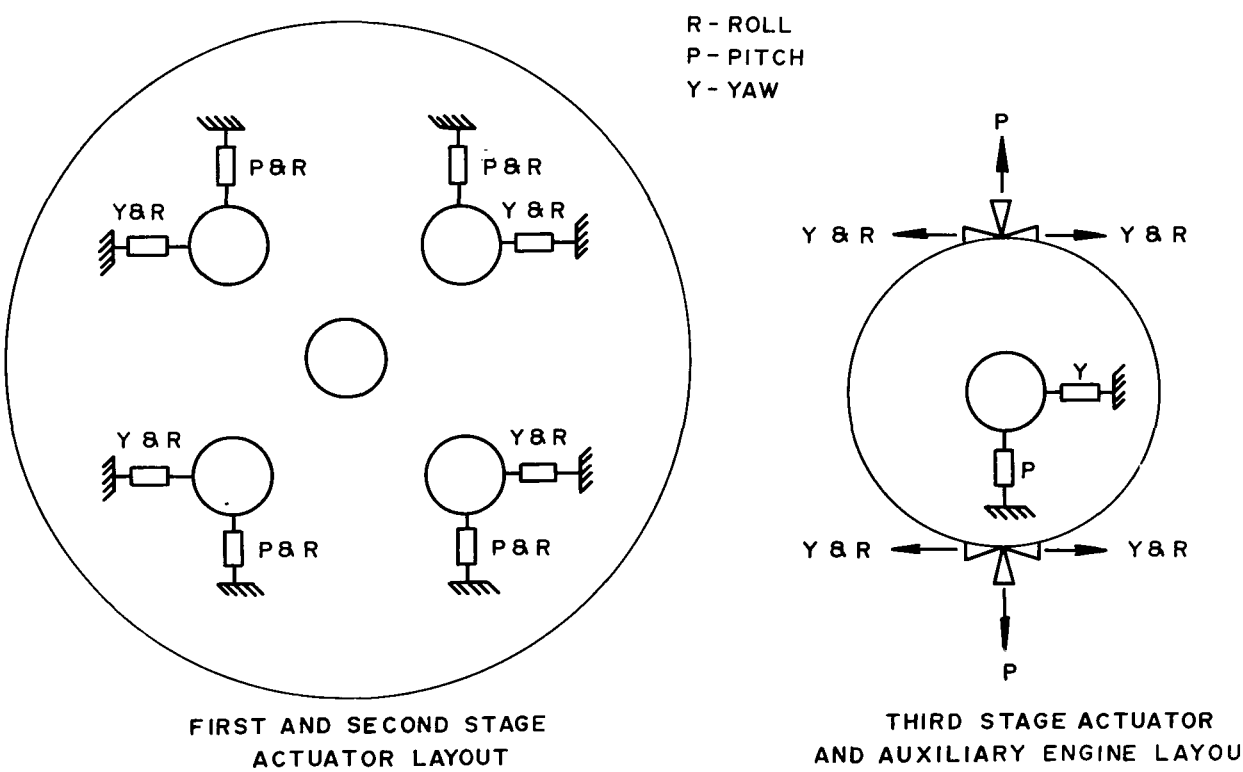

FIGURE 25. ARRANGEMENT OF ACTUATORS.

The signal shaping or filtering of information obtained from the stable platform and rate gyros is performed by passive RC networks. The primary purpose of these shaping circuits is to stabilize the vehicle structural bending either by attenuating the signals of frequencies near the bending modes or by phase shifting them. The frequency response of the filter for the rate gyro output (Fig. 10) is shown in Figure 26. From the Bode plot, it is apparent that the filter will have very little effect in the frequency range of the dominant control mode; however, it supplies sufficient phase lag to stabilize the first bending mode and sufficient attenuation to stabilize all higher bending modes. The filter frequency response for the attitude error signals (Fig. 10) is given in Figure 27. A relatively high static gain is required to achieve adequate control with engine failure, whereas

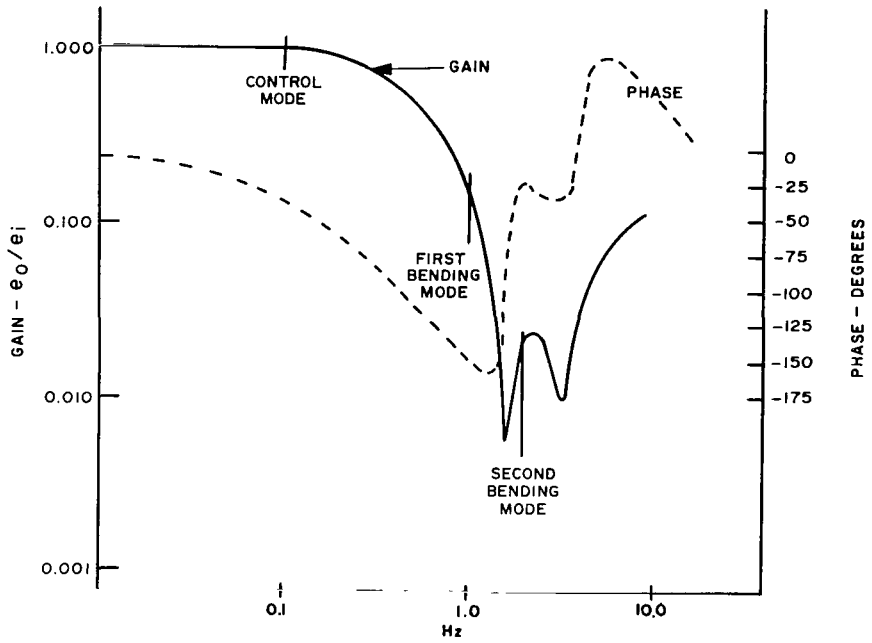

FIGURE 26. FREQUENCY RESPONSE OF THE ATTITUDE RATE SIGNAL FILTER.

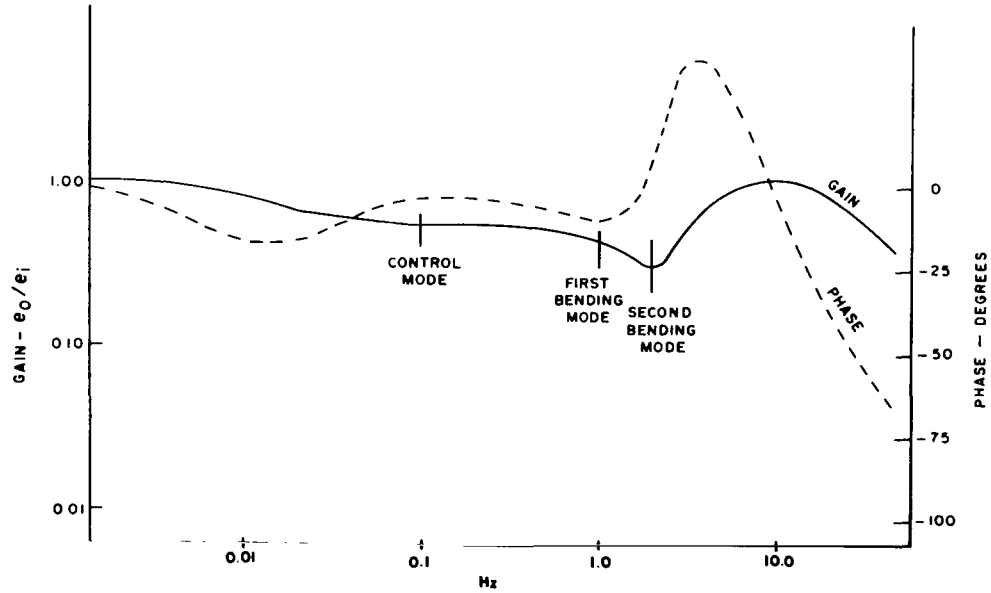

FIGURE 27. FREQUENCY RESPONSE OF THE ATTITUDE ERROR FILTER.

some attenuation is required at the control mode frequency to ensure dynamic stability. The notch located at the second bending mode frequency ensures gain stabilization of this mode.

The modified pitch and yaw input signals are superimposed on the corresponding roll signals as required for individual actuator control by magnetic amplifiers. Since the magnetic amplifiers are current summing devices, the attenuation circuits are simply series resistance. To provide gain factor adaptation, provisions are made for changing this resistance discretely as a function of flight time.

After the signals have been processed in the magnetic amplifiers, transistorized power output stages provide direct current drive to the engine position servos of the first stage; after separation, switchover to the second stage servos occurs. The third stage of the Saturn V has only one control engine and therefore two position servos. Thus six of the servoamplifiers are available to provide a triple redundant driving circuit for each servo.

During coasting periods, the torques needed for attitude control are supplied by an auxiliary propulsion system composed of six small hypergolic rocket engines oriented as shown in Figure 25. The control computer supplies individual firing commands to each of the engines based on a switching scheme designed to minimize fuel consumption. Provisions are made for automatic control or manual control from the Apollo spacecraft. The nonlinear switching characteristics consist of a first order lag circuit in a negative feedback loop around an electronic relay which has variable deadband and hysteresis. All components of the control computer are triple redundant.

Rate gyros

Vehicle angular rates are obtained by use of rate gyros to provide the damping necessary for stabilizing the vehicle control system. The rate information is often achieved by electrically differentiating the analog attitude signal; however, the digital nature of the Saturn attitude reference system does not readily permit electrical differentiation. Also, rate information obtained from a location different from the attitude sensing location may be required to adequately stabilize the vehicle elastic modes.

Two features have been added to the conventional fluid-damped rate gyro for preflight testing. The first is a torquer about the output axis to produce a signal from the microsyn sensor. Excitation of the torquer stimulates signals from the rate gyro output to the control system. The second feature is a gyro speed indicator, consisting of four small permanent magnet slugs symmetrically spaced around the spin motor wheel; the frequency of the voltage induced in a coil located in the gyro housing is a measure of the gyro motor speed.

A triple redundant arrangement with three rate gyros for each of the three vehicle axes has been selected for angular rate measurements in the IU during orbital and injection phases in contrast to the nonredundant rate gyros in the short-life stages.

Thrust-Vector-Control Servoactuators[13]

The angular direction of the thrust vector of high thrust engines (over 0.5×10^6 N) is best controlled by swiveling the gimbal-mounted propulsion engines. This control is obtained by linear hydraulic servoactuators in the pitch and yaw planes.

The actual arrangement of the actuators for the multiengine first and second stages and the single engine stage of the Saturn launch vehicle is shown in Figure 28.

During operation of the rocket engine, the hydraulic power supply is usually provided by a hydraulic pump driven by the engine turbine and an accumulator-reservoir to cover peak loads. An auxiliary pump, driven by an electric motor, provides hydraulic pressure for static checkout of the hydraulic system.

This conventional scheme has been applied for the second and third stage control engines; the hydraulic pressure has been selected conventionally to 2500 N cm^{-2}. For the first stage engines, the hydraulic pressure is received directly from the fuel turbopump at 1400 N cm^{-2}; the fuel is used as hydraulic fluid. The available low operating pressure requires a large servovalve and actuator piston area; however, the pressurization system is very simple and even the accumulator-reservoir can be omitted as a result of the almost unlimited availability of pressurized fuel.

The servoactuators for the Saturn stages have been designed with mechanical feedback to replace the conventional electrical feedback to the driving amplifier located in the control computer. The hydraulic valves employ negative feedback of the actuator piston pressure to reduce actuator resonance resulting from structural compliance and fluid compressibility.

Longitudinal Oscillations (Pogo)[14,15]

The vehicle control sensors are much less sensitive to longitudinal structural modes than to lateral modes. No stability problems have been identified through longitudinal structural modes in conjunction with the control

SIMPLIFIED SYSTEM BLOCK DIAGRAM

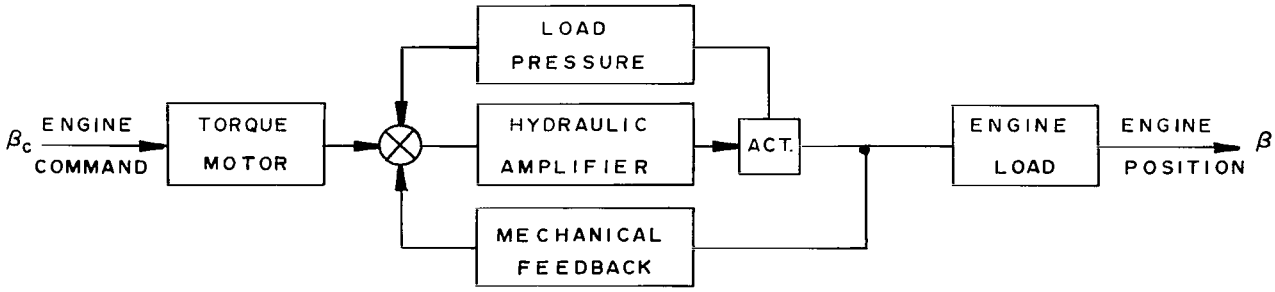

SIMPLIFIED SYSTEM SCHEMATIC

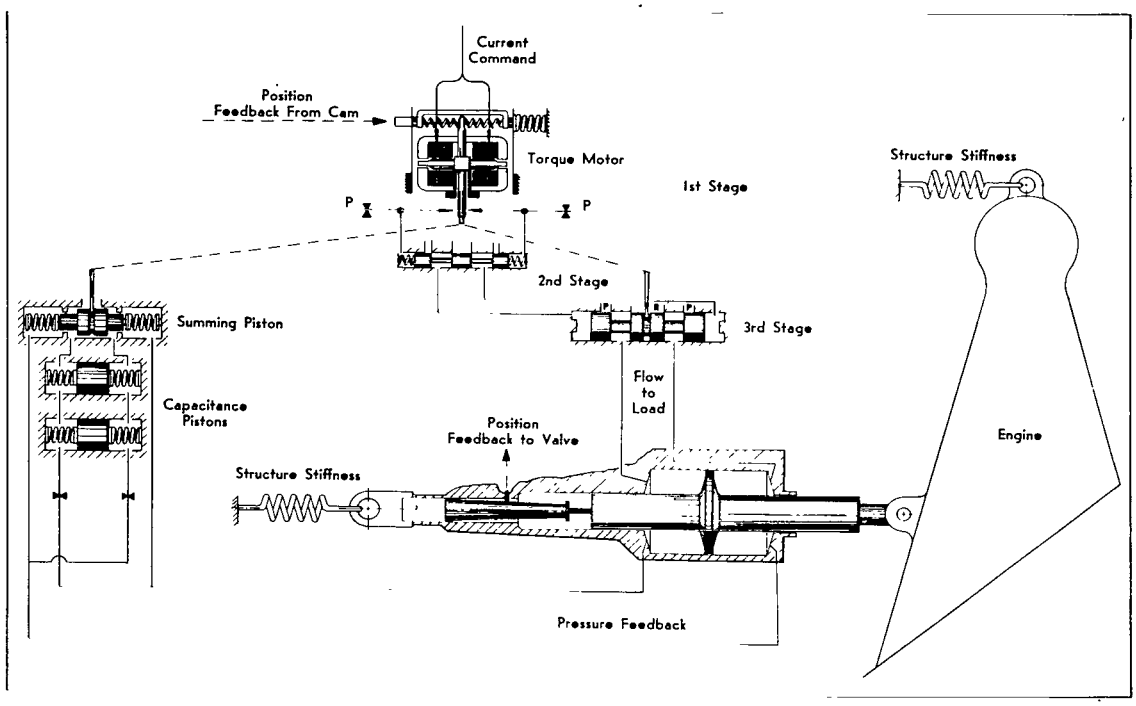

APPROXIMATE LOW FREQUENCY TRANSFER FUNCTION

$$\frac{\beta}{\beta_c} = -\frac{1}{m_2 p^2 + m_1 p + 1}$$

STAGE	m_1	m_2
1	0.047	0.0011
2	0.030	0.0011
3	0.049	0.0017

FIGURE 28. HYDRAULIC ACTUATOR SYSTEM.

system; however, a Saturn V stability problem independent of the control system (commonly called pogo) has been identified. The pogo phenomenon is a divergent longitudinal oscillation (divergence generally limited by nonlinear effects) caused by regenerative feedback of thrust variations through the vehicle structure, propellant tanks, and propellant feed system (Fig. 29).

This problem was first noted as a 5 to 6 Hz oscillation during first stage burn of the first and second Saturn V flights. After an extensive evaluation was made, accumulators were installed on each of the four S-IC outboard engine LOX feedlines prior to the flight of AS-503. Subsequent flights verified the elimination of first stage pogo by these accumulators.

A similar phenomenon existed during the latter part of S-II stage burn after the apparent instability in the S-IC stage had been eliminated. This 16 to 18 Hz S-II pogo was determined to be associated primarily with the center engine and was most predominate near the end of S-II burn. A temporary solution, starting with AS-505, has been to cut off the center engine prior to coalescence of the tank and structural modes. Three possible permanent solutions are presently under evaluation: LOX feedline accumulators, hydraulic damper cylinders between engine mount and thrust structure, and center engine beam stiffening. Preliminary analysis indicates that the use of accumulators is the most promising solution to the problem.

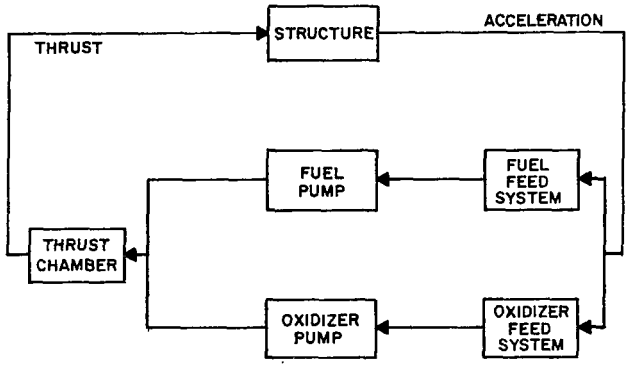

FIGURE 29. BLOCK DIAGRAM OF REGENERATION LOOP OF PROPULSION-GENERATED STRUCTURAL OSCILLATIONS (POGO)

FLIGHT RESULTS OF THE NAVIGATION, GUIDANCE, AND CONTROL SYSTEM

The following information is used in evaluating the accuracy of the navigation, guidance, and control system.

1. The preflight operational trajectory, which would be flown by the vehicle under ideal assumptions, e.g., standard conditions and no perturbations or misalignments.

2. The trajectory derived from telemetered data; the inertial sensor inaccuracies are not contained in these data, but the onboard trajectory computation is included as a function of the inertial sensor information.

3. The actual trajectory, which can be determined in comparison to the preflight and the telemetered trajectories only to a limited accuracy with the presently available tracking methods and techniques, particularly during the propelled flight phases. The accuracy can be improved for certain singular points, such as the earth-orbit injection point or the translunar injection point by extrapolation of a most probable flight path constructed from a high number of tracking data.

The navigation and guidance scheme and its computational implementation are designed to contribute errors approximately one order of magnitude smaller than the expected hardware errors in the total error budget. Thus the following evaluation presents satisfactory knowledge about the performance of the navigation, guidance, and control system under ordinary circumstances.

1. A continuous display of position and velocity deviations (telemetered flight path data minus preflight operational trajectory data) indicates the overall and, in particular, the dynamic performance of the guidance and control system disregarding inertial sensor errors.

2. The velocity vector difference of the singular points evaluated from tracking the actual trajectory and the corresponding points determined by the telemetered onboard computer evaluation exhibits the accuracy of the total navigation, guidance, and control system.

According to these considerations, the following flight results of the Saturn/Apollo lunar missions were derived by subtracting the preflight operational trajectory values from the onboard digital computer data telemetered during flight. R is defined as the radius of the vehicle from the center of the earth and $\dot{R}$ is the rate of change of the radius.

Flight AS-502. — During this flight the thrust of two engines was lost on the S-II stage after about two thirds of its propelled flight. Figure 30 shows the plots of $\Delta\dot{R}$ and ΔR. Even though the iterative guidance mode (IGM) had been designed to accommodate only the loss of the thrust of one engine, Figure 30 indicates that the vehicle very nearly satisfied the altitude constraint. Since that time the IGM has been modified to accept any thrust level that can accommodate the mission.

Figure 31 shows the plots of Δ crossrange velocity and Δ crossrange position. These plots indicate that the vehicle was somewhat out of plane because of the thrust abnormality.

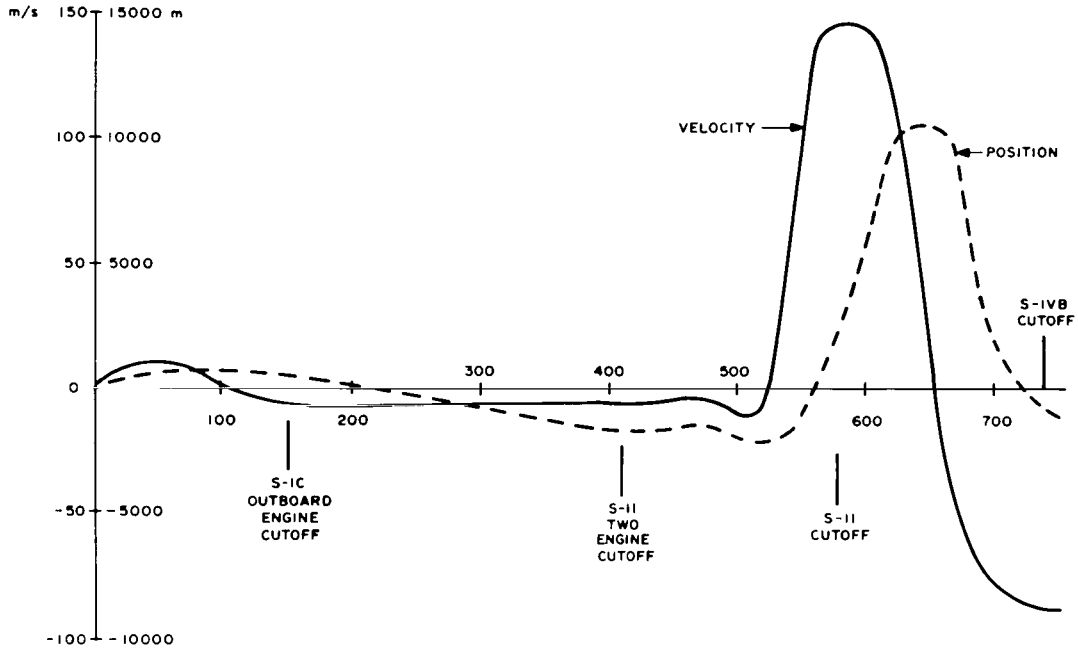

FIGURE 30. $\Delta\dot{R}$ (M/S) AND ΔR (M) VERSUS TIME (S) OF AS-502

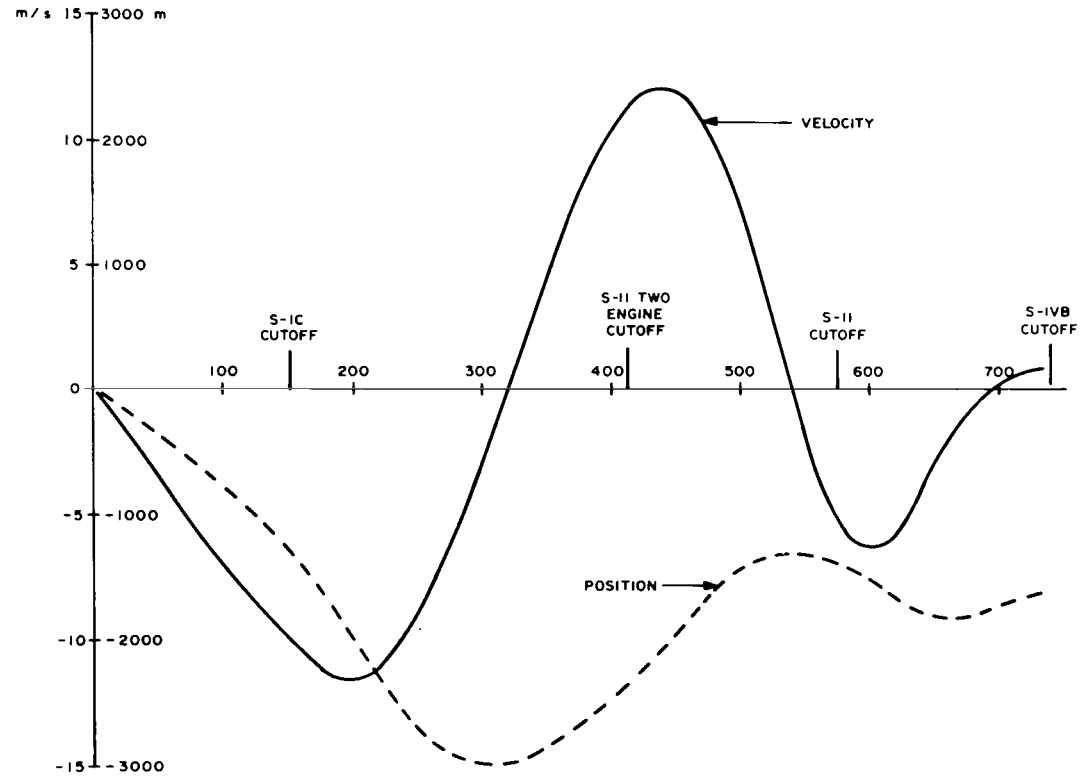

FIGURE 31. $\Delta\dot{Y}$ (M/S) AND ΔY (M) VERSUS TIME (S) OF AS-502

Flight AS-503.— Figure 32 displays $\Delta\dot{R}$ and ΔR during the propelled flight phase up to earth orbit. This figure shows the trend of all the lunar missions in that the vehicle will drift slightly from nominal during the first stage burn and then, upon initiation of guidance, will compensate for this drift and fly to the desired end conditions at insertion.

Plots of $\Delta\dot{R}$ and ΔR from earth orbit to translunar injection are shown in Figure 33. The parameters $\Delta\dot{R}$ and ΔR are not expected to return to zero at cutoff because the digital computer issues the cutoff command based on orbital energy rather than a preset altitude and velocity. These curves are typical for the earth parking orbit to translunar injection portion of all flights; therefore, the corresponding curves are not shown for the following flights.

Plots of Δ crossrange velocity and Δ crossrange position up to earth orbit are shown in Figure 34.

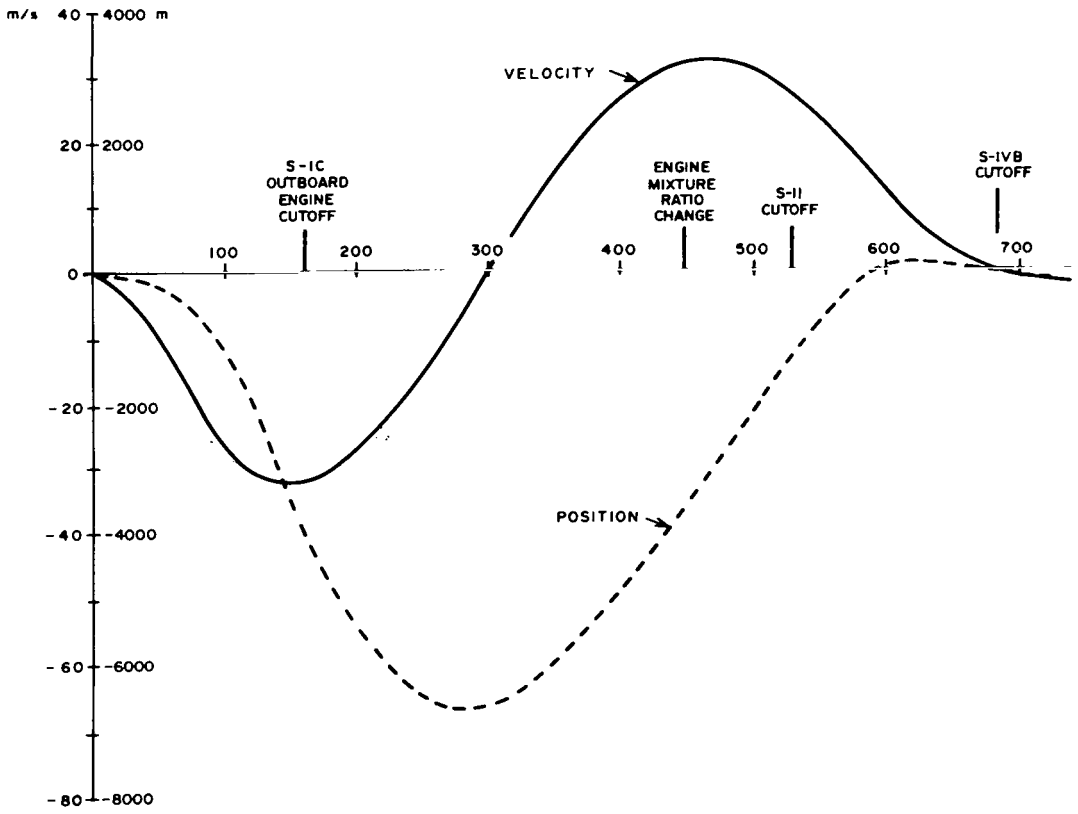

FIGURE 32. $\Delta\dot{R}$ (M/S) AND ΔR (M) VERSUS TIME (S) OF AS-503

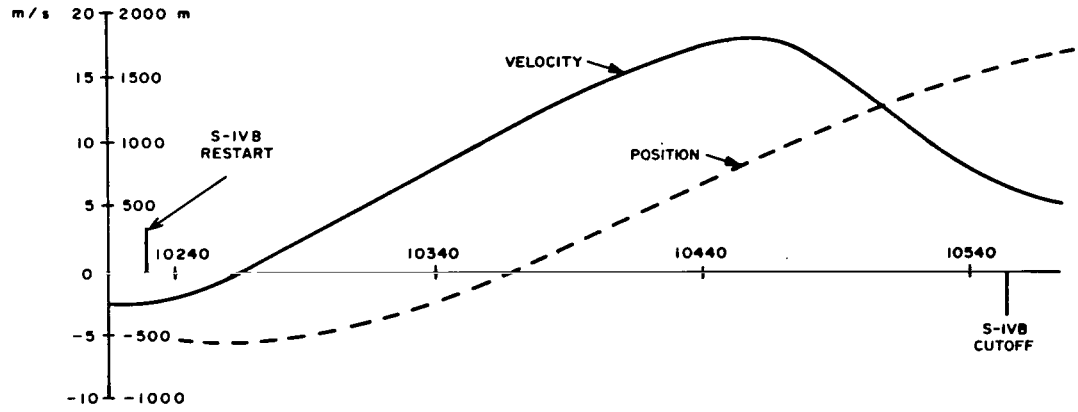

FIGURE 33. $\Delta\dot{R}$ (M/S) AND ΔR (M) VERSUS TIME (S) OF AS-503

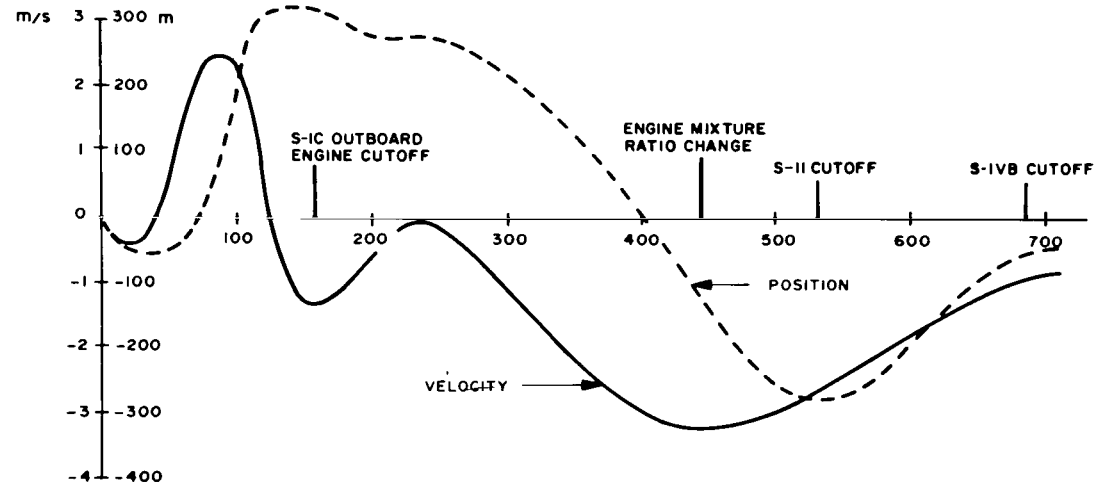

FIGURE 34. $\Delta\dot{Y}$ (M/S) AND ΔY (M) VERSUS TIME (S) OF AS-503.

Flight AS-505.— Figures 35 and 36 are plots of $\Delta\dot{R}$ and ΔR and Δ crossrange velocity and Δ crossrange position, respectively.

Flight AS-506.— The plots shown in Figures 37 and 38 are very similar to those shown for AS-505. One note of interest on Δ crossrange velocity and position (Fig. 38) is that, because of vibration around the Instrument Unit during liftoff, the crossrange accelerometer indicated a false change of -1.6 m/s. This error, however, had no significant affect on the mission.

Flight AS-507.— Figures 39 and 40 are again plots of inflight phase and crossrange data. The main perturbations were caused by a slightly higher than nominal thrust and a lower than nominal velocity ($\Delta V \approx 10$ m/s) achieved by the first stage, a lower than nominal performance of the second stage, and therefore the additional burning time (≈ 4 s) required for the third stage to achieve earth orbit injection (Table 7).

As in earlier flights, the curves indicate excellent dynamic response and very satisfactory orbit injection.

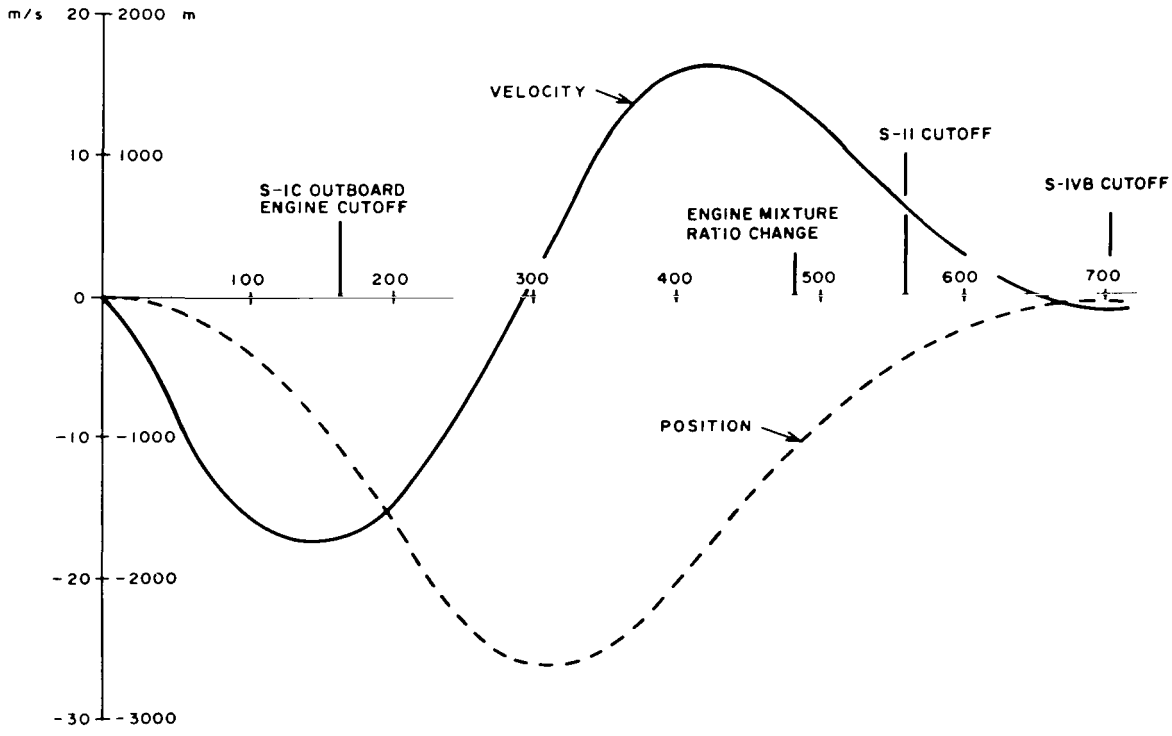

FIGURE 35. $\Delta\dot{R}$ (M/S) AND ΔR (M) VERSUS TIME (S) OF AS-505.

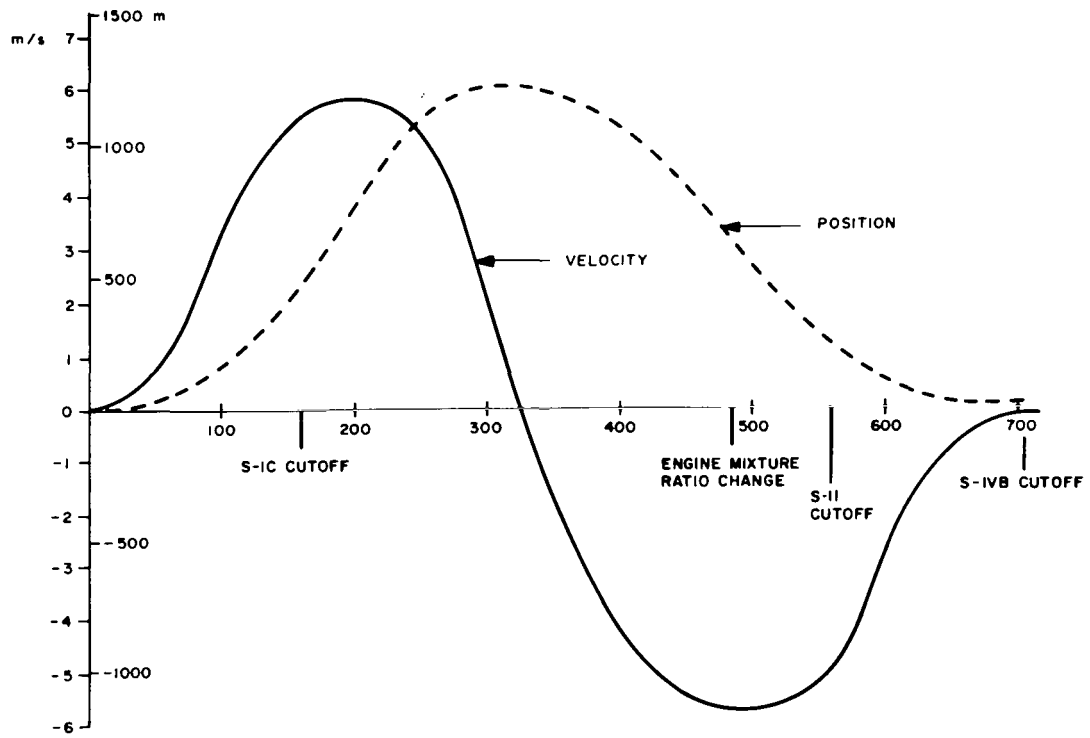

FIGURE 36. $\Delta\dot{Y}$ (M/S) AND ΔY (M) VERSUS TIME (S) OF AS-505.

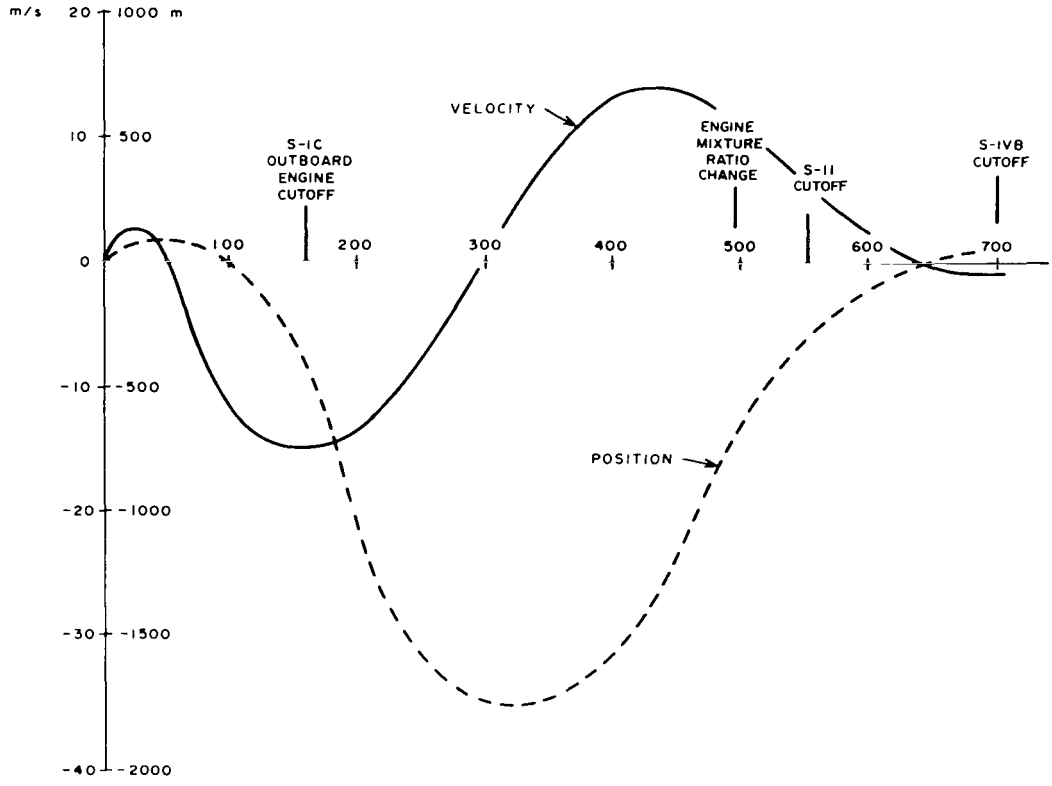

FIGURE 37. $\Delta\dot{R}$ (M/S) AND ΔR (M) VERSUS TIME (S) OF AS-506

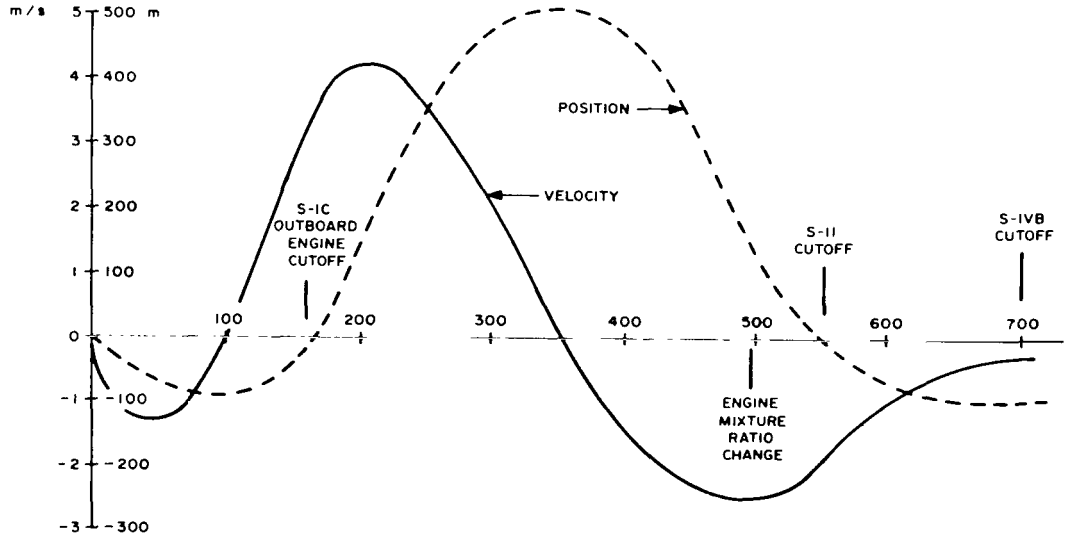

FIGURE 38. $\Delta\dot{Y}$ (M/S) AND ΔY (M) VERSUS TIME (S) OF AS-506.

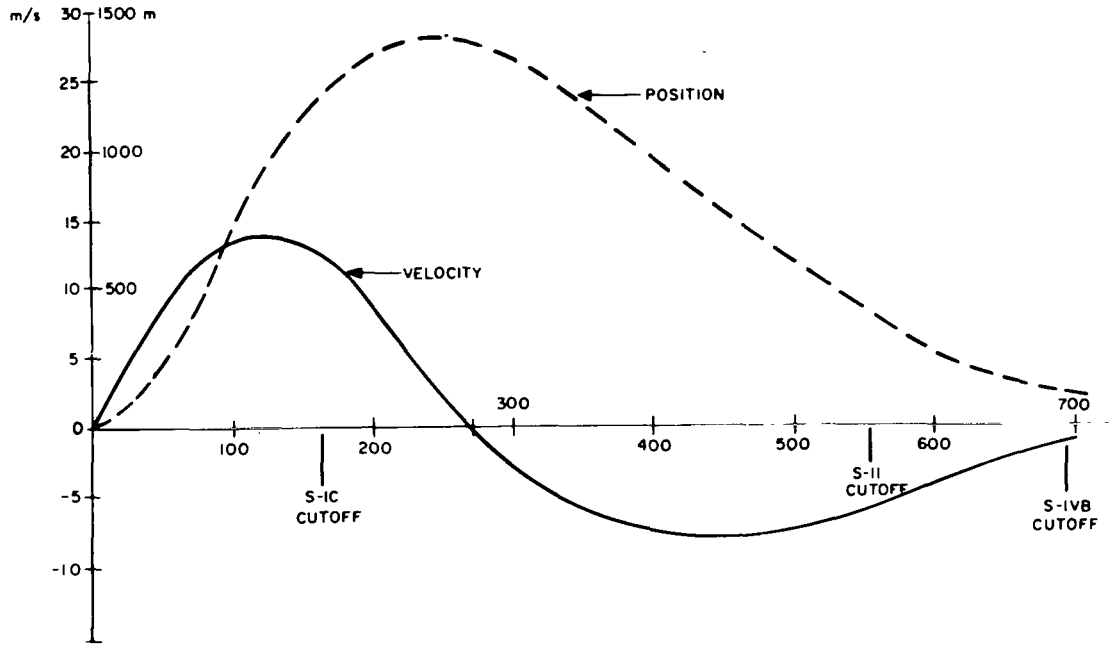

FIGURE 39. $\Delta\dot{R}$ (M/S) AND ΔR (M) VERSUS TIME (S) OF AS-507.

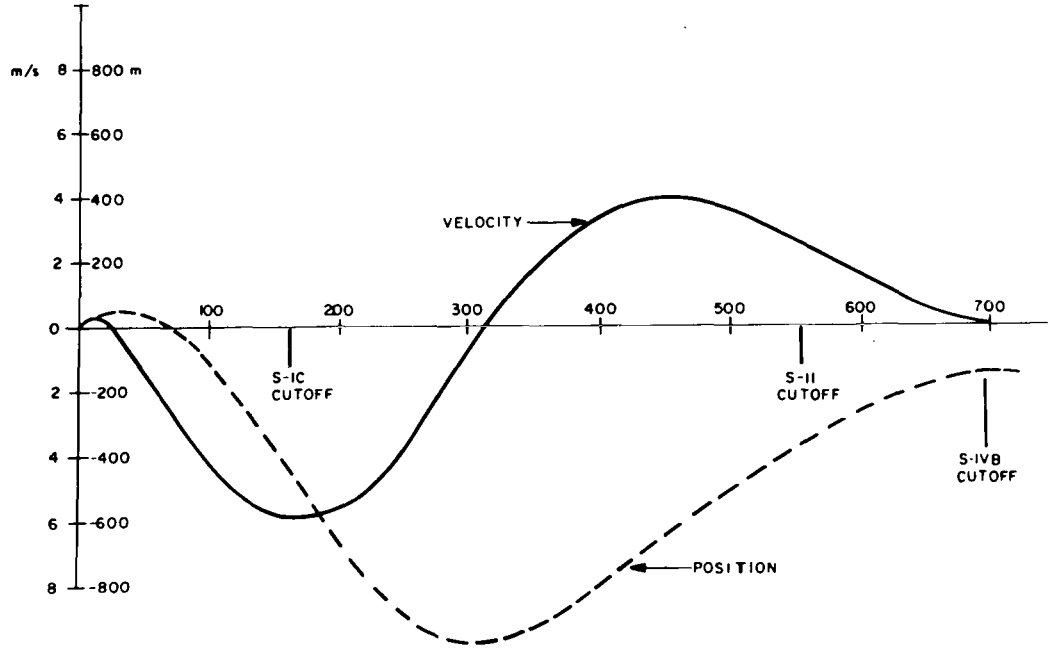

FIGURE 40. $\Delta\dot{Y}$ (M/S) AND ΔY (M) VERSUS TIME (S) OF AS-507.

In the preceding figures, the major point of emphasis is that the IGM successfully guided and controlled the vehicle to the desired end conditions.

Tables 7 and 8 show singular point evaluations for the lunar mission flights AS-503, AS-505, AS-506, and AS-507. In these cases, the small velocity, position, and path angle differences exhibit the excellent performance, particularly in view of accuracy, of the overall navigation, guidance, and control system.

The performance of the onboard hardware has also been excellent with respect to failures. Neither during prelaunch checkout nor during flight have there been any failures of redundant components or parts in the digital or analog subsystems of the navigation, guidance, and control system.

Table 7. Parking Orbit Insertion Performance

Vehicle	Time* (s)	Velocity (m/s)	Radius (m)	Path Angle (deg)
AS-503	0.98	-0.45	50.5	0.0006
AS-505	0.27	0.3	45.2	0.0076
AS-506	-0.16	0.2	285.7	-0.0126
AS-507	4.047	-0.61	475	0.0133

*Actual minus preflight operational flight time difference; all other data are telemetered minus tracking trajectory data.

Table 8. Translunar Injection Performance

Vehicle	Time* (s)	$\dot{X}_S$ (m/s)	$\dot{Y}_S$ (m/s)	$\dot{Z}_S$ (m/s)
AS-503	3.23	-6.9	5.4	5.2
AS-505	0.29	2.1	0.7	5.7
AS-506	-1.05	2.61	-1.80	5.23
AS-507	-1.069	35.2	0.22	-21.5

*Actual minus preflight operational flight time difference; all other data are telemetered minus tracking trajectory data.

ACKNOWLEDGMENT

Acknowledgment for contributions to this report is given to Mr. Melvin Brooks and members of his Guidance and Control Systems Branch, Astrionics Laboratory, MSFC.

George C. Marshall Space Flight Center
National Aeronautics and Space Administration
Marshall Space Flight Center, Alabama
February 1970
933-89-00-0000

REFERENCES

(1) Space Technology, Edited by Howard S. Seifert, John Wiley and Sons, Inc., New York, N. Y., 1959.

(2) Cooper, F. Don: Implementation of the Saturn V Guidance Equations for Lunar Missions from an Earth Parking Orbit, presented at the 12th Flight Mechanics, Dynamics, Guidance and Control Panel Meeting, Manned Spacecraft Center, Houston, Texas, April 13-14, 1965.

(3) Haeussermann, W., and R. C. Duncan: Status of Guidance and Control Methods, Instrumentation, and Techniques as Applied in the Apollo Project, presented at the Lecture Series on Orbit Optimization and Advanced Guidance Instrumentation, Advisory Group for Aeronautical Research and Development, North Atlantic Treaty Organization, Duesseldorf, Germany, Oct. 21-22, 1964.

(4) Haeussermann, W.: Stability Areas of Missile Control Systems, Jet Propulsion, ARS, Vol. 27, p. 787, July 1957.

(5) Hood, B. N.: S-IC/S-II Separation Control Summary Report, S&ID, North American Aviation, Inc., Downey, Calif.

(6) TRW Space Technology Laboratories: Final Report on Saturn V Control System Studies, Contract NAS8-2625, Redondo Beach, Calif., Feb. 28, 1964.

(7) The Bendix Corp.: A Description of the ST124-M Inertial Stabilized Platform and Its Application to the Saturn Launch Vehicle, Eclipse-Pioneer, Teterboro, N. J., May 1964. Presented at the German Rocket Society Symposium, Darmstadt, Germany, June 26, 1964.

(8) Haeussermann, W.: Inertial Instruments with Gas Bearings, Kreiselprobleme Gyrodynamics, IUTAM, Symposium Celerina, Springer-Verlag, Berlin, 1962 (Edited by Hans Ziegler).

(9) Bodie, W. G.: Techniques of Implementing Launch Automation Programs (Saturn IB Space Vehicle System), presented at the 4th Annual Reliability and Maintainability Conference, Los Angeles, Calif., July 28-30, 1965.

(10) Moore, F. B., and J. B. White: Application of Redundancy in the Saturn V Guidance and Control System, AIAA Paper No. 67-553, AIAA Guidance, Control, and Flight Dynamics Conference, Huntsville, Ala., Aug. 1967.

(11) Booth, A. D., and K. H. V. Booth: Automatic Digital Calculators, Academic Press, Inc., New York, N. Y. 1956.

(12) Thompson, Z., and R. J. Alcott: Apollo Booster Flight Control System Integration, presented at the SAE A-18 Committee Meeting, Houston, Texas, Dec. 11-13, 1963.

(13) Kalange, M. A., and V. R. Neiland: Saturn I Engine Gimbal and Thrust Vector Control System, presented at the National Conference on Industrial Hydraulics, Oct. 17-18, 1963.

(14) von Pragenau, George L.: Stability Analysis of Apollo Saturn V Propulsion and Structural Feedback Loop, AIAA Paper No. 69-877, AIAA Guidance, Control, and Flight Dynamics Conference, Princeton, N. J., Aug. 18-20, 1969.

(15) Rich, Roy L.: Saturn V Pogo and a Solution, Proceedings of the AIAA Structural Dynamics and Aeroelasticit Specialist Conference, New Orleans, La., April 16-17 1969.

BIBLIOGRAPHY

(1) Chandler, Doris C., H. J. Horn, and Daniel T. Martin: An Iterative Guidance Scheme and Its Application to Lunar Landing, MTP-AERO-63-11, Marshall Space Flight Center, Huntsville, Ala., Feb. 6, 1963.

(2) Smith, I. E., and E. T. Deaton, Jr.: An Iterative Guidance Scheme for Ascent to Orbit (Suborbital Start of the Third Stage), MTP-AERO-63-44, Marshall Space Flight Center, Huntsville, Ala., May 29, 1963.

(3) Horn, H. J.: Application of an "Iterative Guidance Mode" to a Lunar Landing, presented at the Third European Space Flight Symposium, 15th Annual Meeting of the Deutsche Gesellschaft für Rakententechnik und Raumfahrt e. V., Stuttgart, Germany, May 22-24, 1963.

(4) Smith, Isaac E.: A Three Dimensional Ascending Iterative Guidance Mode, NASA TM X-53258, Marshall Space Flight Center, Huntsville, Ala., May 12, 1965.